A Compound that Inhibits Glycolysis in Prostate Cancer Controls Growth of Advanced Prostate Cancer

Takuma Uo[1,*], Kayode K. Ojo[2†], Cynthia C. Sprenger[1†], Kathryn Soriano Epilepsia[1], B. Gayani K. Perera[3], Mamatha Damodarasamy[1], Shihua Sun[1], Soojin Kim[1], Hannah H. Hogan[1], Matthew A. Hulverson[2], Ryan Choi[2], Grant R. Whitman[2], Lynn K. Barrett[2], Samantha A. Michaels[2], Linda H. Xu[1], Haley J. Pang[1], Matthew M. Nguyen[1], Anna-Lena B.G. Vigil[4], Varun Kamat[5], Lucas B. Sullivan[4, 6], Ian R. Sweet[5], Ram Vidadala[3], Dustin J. Maly[3], Wesley C. Van Voorhis[2,*], Stephen R. Plymate[1, 7*]

Affiliations:

[1]Department of Medicine, Division of Gerontology and Geriatric Medicine, University of Washington; Seattle, Washington 98109, USA.

[2]Department of Medicine, Division of Allergy and Infectious Disease, Center for Emerging and Reemerging Infectious Disease (CERID), University of Washington; Seattle, Washington 98109, USA.

[3]Department of Chemistry, University of Washington; Seattle, Washington 98195, USA.

[4]Human Biology Division, Fred Hutchinson Cancer Center; Seattle, Washington 98109, USA.

[5]Department of Medicine, Division of Metabolism, Endocrinology and Nutrition, Diabetes Center, University of Washington; Seattle, Washington 98109, USA.

[6]Department of Biochemistry, University of Washington; Seattle, Washington 98195, USA.

[7]Geriatrics Research Education and Clinical Center, VA Puget Sound Health Care System; Seattle, Washington 98108, USA.

***** Corresponding Authors

[†] These authors contributed equally to this paper

ABSTRACT

Metastatic castration-resistant prostate cancer remains incurable regardless of recent therapeutic advances. Tumors display highly glycolytic phenotypes as the cancer progresses. In this study, we report the preclinical activity and characterization of a novel series of small molecules with antiglycolytic activity mediated through inhibition of hexokinase 2. These compounds display selective growth inhibition across multiple prostate cancer models. We describe a lead compound (BKIDC-1553) that demonstrates promising pharmacological properties and activity in preclinical models of advanced prostate cancer. This work supports testing BKIDC-1553 and its derivatives in clinical trials for patients with advanced prostate cancer.

Running title: Novel antiglycolytic agents for prostate cancer therapy

Keywords: Cancer metabolism; Prostate Cancer; Glycolysis; Hexokinase; Drug development

INTRODUCTION

Prostate cancer (PCa) is responsible for the deaths of more than 375,000 men worldwide and the second most common solid tumor in men(*1*). Although primary therapies such as surgery or radiotherapy appear to cure many men diagnosed with PCa, the disease becomes incurable once it metastasizes(*2, 3*).

Treatment modalities for PCa have expanded significantly over the past decade with development of potent androgen receptor signaling inhibitors (ARSi) (e.g., abiraterone, enzalutamide)(*2, 4*). Additionally, tumors with loss of function mutations in homologous recombination repair pathway genes (e.g., BRCA1/2) define a subgroup of patients who can benefit from treatment with poly ADP ribose polymerase (PARP) inhibitors and possibly other DNA damaging therapies such as carboplatin(*5*). More recently, radionuclide therapies such as Radium 223 and PSMA targeting with Lutetium 177 have provided new avenues of therapy(*6, 7*). Although these therapies have been demonstrated to improve overall survival, the improvement is incremental, and resistance develops in the majority of cases(*2, 8*). One avenue of therapy for castration-resistant prostate cancer (CRPC) that has yet to realize its full potential involves the development of agents designed to selectively inhibit tumor metabolism(*9, 10*). To date, targeting tumor metabolism, particularly glycolysis or mitochondrial metabolism, has been stymied due to excessive toxicity and/or lack of efficacy(*11*).

Changes to cell metabolism is a hallmark of cancer that drives and supports oncogenesis(*12-14*). Both tumor genetics and tissue context define cancer dependence on specific metabolic pathways, with the tumor ultimately undergoing progression and being driven by combinations of oxidative phosphorylation, glycolysis, and potentially

fatty acid metabolism(*15*). One hundred years have passed since Otto Warburg's pioneering work to report the dominance of aerobic glycolysis in tumors(*16*). Nevertheless, non-specific antiglycolytic agents such as 2-deoxyglucose (2-DG), have never been clinically translated as they not only affect tumor cells but also inhibit normal proliferating cells(*15, 17*).

While glycolysis is not a significant driver in primary PCa, in more aggressive lethal forms of the disease glycolysis is a major driver of tumor progression especially as the tumor has to exist in a hypoxic environment(*18-21*). Challenging our ability to develop drugs against this pathway are multiple enzymatic isoforms in the glycolytic pathway that perform overlapping functions, complicating specific targeting(*15*). Accordingly, flexibility and redundancy among metabolic genes could shape the landscape of positive and negative impact on targeting tumor metabolism(*9, 15*). As far as glycolysis is concerned, isoform specific contribution to tumor progression is exemplified by pyruvate kinase M2 (PKM2) and hexokinase 2 (HK2), where activation and inhibition have been shown to reduce tumor progression, respectively, despite continued expression of corresponding isoforms such as PKM1 and HK1(*22, 23*). HK2 has been reported to be essential for PTEN/p53 deficient CRPC growth(*24*).

Previous protein kinase profiling of bumped kinase inhibitor (BKI) derived compounds (BKIDCs) (BKIDC-1369, 1553, 1561, and 1649) revealed potential human kinase targets, including human receptor-interacting serine/threonine-protein kinase 2 (RIPK2) and protein kinase D (PKD1-3)(*25*). Given that other studies have shown adenocarcinoma prostate cancer (adeno-PCa) cell lines are inhibited by pan-PKD

inhibitors – irrespective of AR status – we set out to screen for cell types that might be affected by BKIDC compounds (*26, 27*).

In this study, we report on the discovery of a novel series of BKIDCs, that display selective inhibition of PCa growth and that are associated with a cessation of glycolysis within 10 min of exposure to the compounds. Herein, we describe a lead compound (referred to as BKIDC-1553) that demonstrates promising pharmacological properties and activity in preclinical models of advanced PCa.

RESULTS

BKIDC effects in Prostate Cancer cell lines

Our lead compound, BKIDC-1553 has oral availability with a favorable safety and pharmacokinetics profile (compound **32** in (*28*)). BKIDC-1553 was tested in the MTS (3-(4,5-dimethylthiazol-2-yl)-2,5-diphenyltetrazolium bromide) assay for proliferation inhibition in a series of human PCa cell lines (LNCaP, LnCaP95, C4-2, C4-2B, LAPC4, VCaP, PC3, DU145, LNCaP^{APIPC}(*29*), MSKCC-EF1 and NCI-H660) and non-prostate control lines (HepG2, U2OS, WIL2-NS and HFF) (**Figure 1A**). From the data we see that androgen receptor (AR) positive lines LNCaP, LNCaP95, C4-2, C4-2B, LAPC4 and VCaP as well as AR negative LNCaP^{APIPC} and the neuroendocrine (NE) lines MSKCC-EF1 and NCI-H660 respond to BKIDC-1553. The concentration to inhibit cell proliferation by 50% ranged from 2.5-20 µM in these cell lines; concentrations achievable in experimental animals without toxicity. No response to BKIDC-1553 is seen in the AR-negative and non-NE PCa lines [PC3 and DU145]. We also saw no response to BKIDC-1553 from non-PCa cell lines including a human bone cancer line

(U2OS), human foreskin fibroblasts (HFF), a lymphoblastoid (WIL2-NS) or hepatoma (HepG2) cell lines (**Figure 1A**). In summary, BKIDC-1553 was active in suppressing the growth of most AR positive and AR negative metastatic PCa cell lines but was not effective in suppressing the growth of normal fibroblast cells or bone, lymphocyte, or hepatocyte derived cancer cell lines.

We next evaluated if PKD was the target of BKIDCs. We first noted that unlike previously reported PKD inhibitors(*26, 27*), BKIDC-1553 lacked activity against PC3, an AR negative and NE negative cell line. To gain insight into the targets of BKIDC-1553, we performed structure–activity relationship studies with small molecules based on pyrrolopyrimidine (PrP) or pyrazolopyrimidine (PP) scaffolds (**Figure 1B**) with LNCaP95 and PC3 as a representative of responders and non-responders, respectively (**Table S1 and S2**). A series of compounds with variable R1 and R2 substituents still displayed antiproliferative activity in LNCaP95 but not PC3 (**Figure 1C**). We created BKIDCs, represented by BKIDC-1553-N-Me that contain substituents (alkyl groups on the exocyclic nitrogen of pyrimidine) that disrupt canonical hinge region hydrogen bonding interactions in the ATP-binding site of protein kinases (**Figure 1B**). The protein targets of BKIDC-1553-N-Me were determined with competitive proteomic profiling experiments and no protein kinases, including PKD and RIPK2, were identified as hits (**Figure S1**). Yet, BKIDC-1553-N-Me maintained its antiproliferative activity against LNCaP95 (**Figure S2**). This demonstrated PKD and RIPK2 were not BKIDC targets and suggested the antiproliferative actions of BKIDCs on PCa cells acts via a mechanism not requiring protein kinase inhibition.

Indeed, we confirmed that BKIDC-1553-N-Me showed a similar antiproliferative spectrum across the cell lines tested with BKIDC-1553 (**Figure S2**). In this screen, we also found a closely-related molecule, BKIDC-1817 (**Figure 1B**: a 1H-pyrazolo[3,4-d]pyrimidin-4-amine compound)(*30*), had no inhibitory activity in LNCaP95 or PC3 cells (**Figure S2**). BKIDC-1817 served as a negative control in subsequent studies.

BKIDC effects on cell cycle and cell-signaling pathways

We carried out a series of experiments to characterize cell cycle effects, cell-signaling pathways, and energy sources to investigate the cellular processes inhibited by BKIDC-1553 and -1553-N-Me. Thirty-hour exposure to BKIDC-1553 and 1553-N-Me commonly resulted in G1 cell cycle arrest of responders (LNCaP and LNCaP95), but not a non-responder line (PC3) which had no enrichment of the G1 population (**Figure 2A, Figure S3A**). In addition, our negative control BKIDC-1817 did not affect the cell cycle of any cell line. Similar patterns of cell cycle profiles were observed at 48- and 72-h time points with no obvious appearances of the sub-G1 population in LNCaP95 (*31*)(**Figure S3B**), suggesting that cytostatic rather than cytopathic actions of BKIDCs are responsible for their antiproliferative activities.

Since G1 but not G2/M arrest was dominantly associated with BKIDC-induced changes in cell cycle profiles, we took advantage of reverse-phase protein arrays (RPPA) to characterize robust biochemical alterations leading to G1 cell cycle arrest(*32*) (**Figure 2B and 2C, Figures S4 and S5, Table S3**). This high-throughput antibody-based targeted proteomics platform allowed us to observe a time- and dose-dependent decrease in phosphorylated ribosomal protein S6 at serine 235/S236 (P-RPS6$^{S235/S236}$)

and serine 240/S244 (P-RPS6$^{S240/S244}$) in LNCaP95 but not PC3 cells as early as 4 h after treatment with BKIDC-1553 and 1553-N-Me (**Figure 2C, Figure S5**). RPS6 is a canonical downstream target of mTORC1 kinase which is negatively regulated by the metabolic sensor AMP-activated protein kinase (AMPK)(*33, 34*). Indeed, antiproliferative BKIDC-1553-N-Me, but not our negative control BKIDC-1817, consistently activated AMPK in LNCaP95 cells as reflected by increased enzymatic activity and increased phosphorylation of acetyl-CoA carboxylase (ACC) at Ser79 (the major substrate for AMPK)(*33*) (**Figure 3A and 3B**).

We next performed an in vitro enzyme assay using purified human AMPKα1β1γ1 complex to examine whether BKIDC-1553 and 1553-N-Me could be direct activators of AMPK. A well-established allosteric activator A-769662 caused 2-fold increase in AMPK activity (*35*) while BKIDCs failed to do so, suggesting BKIDCs do not stimulate AMPK activity directly (**Table S4**).

Since AMPK serves as a cellular sensor of ATP-ADP-AMP balance in cells, the alteration in ATP metabolism could be upstream of pathways that affect ATP levels and produce AMPK activation(*33*). We examined BKIDC's effects on ATP supply from two major pathways, glycolysis in the cytosol and oxidative phosphorylation (OXPHOS) in mitochondria. OXPHOS inhibition, which was achieved by oligomycin (inhibitor for F0 component of H^+-ATP-synthase) or antimycin A (AA: inhibitor for complex III)(*36*), cooperated with BKIDCs to deplete intracellular ATP (**Figure 3C, Figure S6**). This suggested that BKIDCs inhibit glycolysis-derived ATP production, and indeed a similar effect was seen with the glycolysis inhibitor 2-deoxyglucose (2-DG). Also, similar to 2-DG, BKIDC-1553 and -1553-N-Me cooperated with oligomycin to exhibit cytopathic,

apoptotic actions in LNCaP as judged by increased PARP cleavage and cytolysis(*31*) (**Figure 3D**). Thus, the evidence suggests that BKIDCs interrupt glycolysis, in a way similar to 2-DG.

BKIDC effects on glycolysis

To examine the effects of BKIDCs on glycolysis directly, we employed the Seahorse assay to measure the extracellular acidification rate (ECAR), a proxy for glycolysis rate in cells(*37*). ECAR was suppressed by BKIDCs in LNCaP and LNCaP95 cells but not in BKIDC non-responder cell lines, including DU145, PC3, and U2OS (**Figure 4A and 4B, Figure S7**). Mitochondrial respiration as judged by oxygen consumption rate (OCR) (*38*) was not affected by BKIDC-1553-N-Me in both responder (LNCaP, LNCaP95) and non-responder cell lines (PC3, DU145)(**Figure S7**). The rapid decrease in ECAR with BKIDCs suggests that BKIDCs have a direct anti-glycolytic effect (**Figure 4C**). Under the same conditions, BKIDCs induced a moderate compensatory increase in the oxygen consumption rate (OCR) in LNCaP lines, suggesting aerobic, mitochondrial oxygen consumption partially compensates for inhibition of glycolysis.

In order to determine which glycolytic step is interrupted by BKIDCs, we performed a metabolic flux assay with D-[U-^{13}C] glucose(*39*) (**Figure 5**). We exposed cells to labelled glucose with different concentrations of BKIDC-1553-N-Me and DMSO as a solvent control for 30 min. We did not see significant changes in glucose levels among cells lines and treatment. In LNCaP and LNCaP95 cells, we clearly saw a decrease in the levels of 6 carbon sugar phosphate which includes glucose 6-phosphate and fructose 6-phosphate. Consistently we observed marked reduction in

levels of downstream metabolites, including dihydroxyacetone phosphate (DHAP), phosphoglycerate (PG), phosphoenolpyruvate (PEP), and pyruvate (**Figure 5B**). Importantly, the non-responder cell line DU145 did not display such metabolic alterations. These experiments suggested that either glucose uptake or glucose phosphorylation were affected by BKIDC exposure in susceptible PCa cells(*36*). Supporting this, results from the Glucose Uptake-Glo Assay also were consistent with BKIDC-1553-N-Me blocking glucose uptake and/or phosphorylation (**Figure S8A**).

To distinguish between glucose uptake and glucose phosphorylation steps, we used two different radiolabeled glucose analogs, [^{3}H] 2-DG and [^{3}H] 3-O-methyl D-glucose (3-OMG), which are taken up into cells in the same manner as glucose (**Figure 6**). 2-DG undergoes phosphorylation to become trapped and accumulates in the cells as a form of 2DG-6P. On the other hand, 3-OMG cannot be phosphorylated and its intracellular levels reflect the cell's capability of glucose uptake alone(*40*). We confirmed time-dependent accumulation of 2-DG signals in both LNCaP and DU145 (**Figure S8B**). This accumulation was inhibited by the presence of BKIDC-1553-N-Me in LNCaP but not DU145 cells. BKIDC-1553-N-Me did not inhibit 3-OMG uptake in LNCaP cells, suggesting that BKIDC inhibits the glucose phosphorylation step, not glucose uptake, in BKIDC susceptible cells (**Figure 6B**).

Hexokinases carry out the phosphorylation of glucose and we wanted to learn if BKIDCs were dependent on a specific isoform of hexokinase (HK). Among five isoforms of hexokinases expressed in humans (HK1, HK2, HK3, GCK1/HK4, and HKDC1)(*41*), HK1 and HK2 are reportedly predominant in LNCaP cells(*42*). We used a CRISPR-Cas9 system to generate HK1 and HK2 knock-out (KO) LNCaP clones. We

successfully established several independent HK1 and HK2 KO clones, demonstrating that HK1 and HK2 are dispensable, and deletion of each gene did not affect cell proliferation and survival (**Figure 7 and Figure S9**). We then characterized their sensitivity to BKIDCs. We evaluated intracellular ATP levels, in the presence of oligomycin (OXPHOSi), to determine BKIDC's antiglycolytic activity in the HK1 and HK2 KO lines. Like the parental LNCaP line, individual HK1 KO clones were sensitive to both BKIDC-1553 and 1553-N-Me, demonstrating lower ATP levels in the presence of oligomycin. In sharp contrast, HK2 KO clones displayed remarkable resistance to antiglycolytic action of BKIDCs, in that ATP levels were not suppressed in the presence of oligomycin. Pooled KO lines with different sgRNAs also displayed resistance to BKIDC only with HK2 KO pools, but not with HK1 KO (**Figure S9**). This suggested that BKIDCs exert their antiglycolytic activity through HK2, but not HK1, in susceptible PCa cell lines. Collectively, these findings implicate HK2-mediated glucose phosphorylation as the primary target of BKIDC. An unexpected finding was that both HK1 and HK2 KO clones retained antiproliferative sensitivity to BKIDCs (**Figure S10**). This suggests that BKIDCs may exert antiproliferative effects beyond effects on glycolysis. But from these experiments, it is clear that BKIDCs require HK2, but not HK1, for their effects on ATP generation from glycolysis.

BKIDC effects in preclinical mouse xenograft models

Finally, we tested the therapeutic potential of BKIDC-1553 two in vivo preclinical PCa models. The slow clearance of BKIDC-1553 from the systemic circulation of mice led to exposures of over 2 μM for an extended period of up to 72 h post-dose, which allowed a

Monday, Wednesday, Friday dosing regimen (data not shown). BKIDC-1553, administered 20 mg/kg orally, 3 times/week, decreased tumor growth after 5 weeks in a human LuCaP patient-derived xenograft (PDX), LuCaP 35 (*43*) while PC3 tumors derived from adeno-PCa cell-line derived xenografts were resistant to BKIDC-1553 (**Figure 8**). Intratumoral concentrations of BKIDC-1553 48 h after the end of dosing were similar in PC3 and LuCaP 35 tumors (about 8 µM, **Table S5**), ruling out that observed drug resistance of PC3 is due to low exposure to BKIDC-1553. Importantly, antitumor activities of BKIDC-1553 were comparable to those of standard ARSi enzalutamide treatment in AR+ LuCaP 35 model. These observations are consistent with our in vitro studies and may reflect the association of anti-glycolytic action of BKIDC-1553 with antitumor activity. These results demonstrate that BKIDC-1553 has good systemic exposure and tissue penetration needed to achieve therapeutic levels. Taken together, these xenograft studies suggest BKIDC-1553 could be developed as a safe and effective the therapy of advanced PCa.

DISCUSSION

Despite considerable efforts, precision oncology in advanced PCa has faced challenges, including drug resistance and limited populations who benefit from the related therapeutics(*8*). Metabolic reprogramming is observed in emergent CRPC after initial therapies fail(*44*). In particular, emergent CRPC becomes highly glycolytic as demonstrated by positive ^{18}F-fluorodoxyglucose (^{18}F-FDG) labeling in metastatic CRPC but not primary PCas(*45-47*). Strong avidity to FDG in advanced PCa suggests that targeting glycolysis would have a major impact on PCa progression and would be

especially important in treating those tumors that currently are untreatable or have limited potential treatments(*48*).

However, the therapeutic targeting of metabolic complexes or enzymes in glycolysis is challenging, affecting not only tumor cells but also normal proliferating cells. Multiple enzymatic isoforms can also perform overlapping functions, and metabolic flexibility can divert processes away from inhibited pathways. Mammals possess five HK isoenzymes, including HK1, HK2, HK3, HK4/GCK1, and HKDC1 with overlapping and specific tissue and cellular distribution patterns to fix glucose as the first step in glycolysis(*41*). Along with catalytic domains, HK1 and HK2 contain N-terminal motifs to interact with VDAC1 for association with mitochondria and the glucose-6-phosphate (G6P)-binding sties for feedback allosteric inhibition(*41*). HK2 is required for oncogenic transformation and progression of some cancers, but HK2 is minimally expressed in most adult tissues and its systemic deletion in adult mice does not lead to overt side effects(*22*). Thus, HK2 garners much attention as an ideal and selective target in cancer therapeutics(*49, 50*). Target-based screening has identified HK2 selective inhibitors that competitively or allosterically inhibit catalytic functions or promote dissociation from the mitochondria, though they are still in early phases of clinical development(*51*).

As demonstrated here, using phenotypic screening and target deconvolution, we identified a series of compounds that fulfil a major unmet need for development of metabolism-based therapeutic interventions(*15*). It is clear from Seahorse ECAR measurements that BKIDCs interrupt glycolysis almost immediately after exposure in susceptible PCa cells. This is accompanied by a rapid reduction in glycolysis

metabolites. Experiments showed that 2-DG accumulation, but not 3-OMG accumulation, was interrupted by BKIDCs. This demonstrated that hexokinase activity, but not glucose importation, was targeted by BKIDCs. Finally, knockout of HK2, but not HK1, abrogated the reduced ATP levels observed with BKIDCs combined with oligomycin. This demonstrated that BKIDCs interrupt ATP generation by glycolysis, and appear to do so in a HK2 dependent fashion. This makes sense, in that PCa is known to activate HK2 expression and become dependent on it for glycolysis(*24*).

We explored whether HK2 could be directly targeted by BKIDCs. We were unable to demonstrate that BKIDCs inhibit human recombinant HK2 (hrHK2) enzymatic activity, in phosphorylation of glucose to glucose-6-phosphate (**Figure S11**). This suggests that BKIDCs do not act directly on HK2, but could act on the many molecules that are known to modulate HK2 function(*52*).

As noted, both HK2 and HK1 KO cell lines retained sensitivity to antiproliferative effects of BKIDCs. Observed antiproliferative phenotypes may reflect polypharmacological effects of BKIDCs. Indeed, it is still a matter of debate whether HK2 inhibition is sufficient to elicit antitumor activity(*24, 53-56*). HK1 and HK2 are dispensable in LNCaP cells as knockout of each gene did not affect cell proliferation and survival (this study) (*54*). However, metabolic reprogramming of the HK1 or HK2 KO population may change the coupling of glycolysis to antiproliferative effects. The lack of effect on proliferation may be due to BKIDC effects on other targets or may reflect the plasticity of PCas, allowing them to continue proliferation after complete KO of HK2(*57, 58*).

BKIDCs elicit cell-cycle arrest and AMPK activation, presumably due to the integrated stress response(*59*). As we demonstrated here, BKIDCs synergize with OXPHOS inhibition (oligomycin) to promote cell death. A similar effect to BKIDCs could be seen with the nonspecific glycolysis inhibitor, 2-DG. However, BKIDCs did not exhibit the toxicity to multiple cell lines that 2-DG demonstrates, making BKIDCs a good candidate for clinical therapy. HK2 inhibition reportedly renders therapeutic vulnerability to interference with OXPHOS or glutamine metabolism(*60-62*). This warrants exploration of synthetic lethal pairings for metabolism-targeted combined therapies to improve clinical results of BKIDC actions.

In summary, we overcame the hurdle of targeting tumor metabolism by developing a series of druggable small molecules, BKIDCs, that elicit antiproliferative effects selectively in PCa models. BKIDCs rapidly shut down glycolytic energy production, an effect that appears dependent on HK2 expression.

MATERIALS AND METHODS

Study Design

The goal of this study was to define a mechanism of action of novel small molecules called BKIDCs and their preclinical relevance in prostate cancer therapeutics. This objective was accomplished by (i) finding antiproliferative actions of BKIDCs in prostate cancer cell lines, (ii) characterizing Structure Activity Relationship of BKIDCs, (iii) using cell-based biochemical, bioenergetic, metabolic flux, and radiometric assays to characterize antiglycolytic activities of BKIDCs, and (iv) conducting in vivo preclinical trials delineating the therapeutic efficacy of BKIDC-lead 1553. For in vivo studies, mice

were randomly assigned to each treatment group. The numbers of replicates are specified within each figure legend.

Cell culture

LNCaP, C4-2, C4-2B, VCaP, DU145, PC3, HepG2, HFF, and lymphoblastoid WIL2NS were obtained from the American Type Culture Collection (ATCC). LAPC4 was obtained from Dr. Charles Sawyers (Memorial Sloan Kettering Cancer Center, New York NY), U2OS cells from Dr. Raymond Monnat (University of Washington), NCI-H660 and LNCaP^{APIC} from Peter Nelson (Fred Hutchinson Cancer Center, FHCC)(*29*), LNCaP95 from Alan Meeker (Johns Hopkins University), MSKCC EF1 derived from the organoid line MSKCC-CaP4(*63*) from John K. Lee (FHCC). Cells were maintained in RPMI 1640 (LNCaP, C4-2, C4-2B, DU145, PC3, MSKCC EF1, HepG2, WIL2NS), DMEM (VCaP, U2OS, HFF), and IMDM (Iscove's Modified Dulbecco's Medium, LAPC4) supplemented with 5% fetal bovine serum (FBS), 100 units/ml penicillin, and 0.1 mg/ml streptomycin. LNCaP95 cells were grown in RPMI medium supplemented with 5% charcoal stripped serum. NCI-H660 was cultured in HITES medium (RPMI 1640 medium plus 5 µg /ml insulin, 10 µg /ml transferrin, 30 nM sodium selenite, 10 nM hydrocortisone, 10 nM β-estradiol) with 10% FBS. All cell lines were routinely tested for mycoplasma contamination with Universal Mycoplasma Detection Kit (ATCC).

Metabolomic flux assay

LNCaP95, LNCaP, and DU145 cells were plated at 500 K cells per well on 6-well plates coated with poly-D-lysine (PDL) overnight in media containing unlabeled 10 mM D-

glucose and 2 mM L-glutamine. Cells were treated in triplicate with drug or vehicle for 30 min. Cells were then quickly washed two times with RPMI media with L-glutamine and without glucose. Media was then changed to fresh RPMI with 10 mM [U]^{13}C-glucose (Cambridge Isotope Laboratories) and unlabeled 2 mM glutamine in the presence of different concentrations of BKIDC-1553-N-Me. DMSO was used as vehicle control. Cells were then harvested 30 min after treatment with [U]^{13}C-glucose and inhibitors.

Cells were then quickly washed twice with ice cold blood bank saline and quenched with 500 µl HPLC-grade 80% methanol containing 2.5 µM valine D8 extraction standard. Samples were then centrifuged at 4°C at 17,000 g for 5 min. 400 µl of supernatant was transferred to a new microfuge tube and centrifuged at 4°C at 17,000 g for 5 min. 350 µl of supernatant was then transferred to a new microfuge tube and dried down with a Labonco Centrivap Centrifugal Vacuum Concentrator at 4°C and placed at -80°C until time of analysis. Samples were then re-constituted with 50 µl of 80% HPLC-grade methanol, vortexed for 10 min at 4°C, and centrifuged at 17,000g for 5 min at 4°C. 40 µL of supernatant was transferred to a liquid chromatography-mass spectrometry (LC-MS) vial for measurement by LC-MS. Metabolite quantitation was performed using a Q Exactive HF-X Hybrid Quadrupole-Orbitrap Mass Spectrometer equipped with an Ion Max API source and H-ESI II probe, coupled to a Vanquish Flex Binary UHPLC system (Thermo Scientific). Mass calibrations were completed at a minimum of every 5 days in both the positive and negative polarity modes using LTQ Velos ESI Calibration Solution (Pierce). Samples were chromatographically separated by injecting a sample volume of 1 µl into a SeQuant ZIC-pHILIC Polymeric column (150

x 2.1 mm 5 µM, EMD Millipore). The flow rate was set to 150 µl/min, autosampler temperature set to 10 °C, and column temperature set to 30°C. Mobile Phase A consisted of 20 mM ammonium carbonate and 0.1% (v/v) ammonium hydroxide, while Mobile Phase B consisted of 100% acetonitrile (ACN). The sample was gradient eluted (%B) from the column as follows: 0-20 min.: linear gradient from 85% to 20% B; 20-24 min.: hold at 20% B; 24-24.5 min.: linear gradient from 20% to 85% B; 24.5 min.-end: hold at 85% B until equilibrated with ten column volumes. Mobile Phase was directed into the ion source with the following parameters: sheath gas = 45, auxiliary gas = 15, sweep gas = 2, spray voltage = 2.9 kV in the negative mode or 3.5 kV in the positive mode, capillary temperature = 300 °C, RF level = 40%, auxiliary gas heater temperature = 325°C. Mass detection was conducted with a resolution of 240,000 in full scan mode, with an AGC target of 3,000,000 and maximum injection time of 250 msec. Metabolites were detected over mass range of 70-1050 m/z in full scan mode with polarity switching. Quantitation of all metabolites was performed using Tracefinder 4.1 (Thermo Fisher Scientific) referencing an in-house glycolytic metabolite standards library using ≤ 5 ppm mass error.

Glucose uptake assay

Luciferase-based assay: LNCaP cells were plated at 240 K cells/well in PDL-coated 24-well plates. 24 h later, medium was changed to serum and glucose-free medium containing BKI at 20 µM or cytochalasin B (CytB) at 20 µM for 30 min prior to the experiment. Cells were then rinsed and incubated media containing 2DG and BKI or CytB for 10 min. Glucose uptake was measured using the Glucose Uptake-Glo™ Assay

(Promega®) according to the manufacturer's protocol. This luciferase-based assay measures 2-DG-6-phosphate (2-DG-6-P) which accumulates as a dead-end product after hexokinase-mediated conversion of 2-DG. Either BKIDC-1553-N-Me or CytB was added after cellular harvest, to demonstrate these compounds did not interfere with the assay to evaluate 2-DG accumulation. The data were presented as mean relative luminescence units (RLU) ± standard deviation (SD) (n=3).

Radiometric assay: Uptake of ^{3}H-3-O-methylglucose (American Radiolabeled Chemicals, St. Louis, MO) and ^{3}H-2-deoxyglucose (Perkin Elmer, Waltham, MA) was measured as carried out previously(*40, 64*). Cells were incubated in 12 x 75 mm polypropylene test tubes containing Krebs-Ringer bicarbonate solution (KRB) (with 5 mM bicarbonate and 0.1% BSA) at 37°C for 30 min in a shaking water bath. Cell densities were 2 x10^{6} cells per 200 µL for all cell types. Radiolabeled molecules (0.175 µCi) were added to the tubes using an Eppendorf Repeater pipet and the cells were further incubated in the presence of a radiotracer for 30 min. (Supplemental experiments carried out showed that between 10 and 30 min, uptake of tracer was linear (data not shown)). The specific activities and the concentrations in the incubation media of the radiotracers were as follows: [^{3}H]3-O- MG, 90 Ci/mmol, 24 nM; [^{3}H]2-deoxyglucose, 20 Ci/mmol, 119 nM. Accumulation of radiolabel was determined by separating the cell-associated radioactivity (CAR) from the free radioactivity by transferring the cell suspension to a 0.4 mL centrifuge tube (USA Scientific, Ocala, FL) containing a layer of oil consisting of 1:37.5 n-dodecane:bromo-dodecane (Sigma–Aldrich, St. Louis, MO) and spinning at 12,535 g for 8 s (Beckman E centrifuge,

Beckman Coulter, Fullerton, CA). The tube was placed briefly in liquid nitrogen, cut through the radioactive-free oil layer with a razor blade, and the bottom portion of the tube containing the cell pellet was placed into a 7 mL glass scintillation vial. The ^{3}H labels were counted using a Beckman liquid scintillation counter (Model LS6500) after adding 5 ml of Ecolume liquid scintillation cocktail (MP Biomedicals, Cat No. 0188247001) and vortexing the vials. Values of non-specific association of radioactivity was determined by performing the assay in the presence of 5 mM glucose at 4°C. The CAR data for each sample was normalized by subtracting off the non-specific values, and then dividing by the cell number and the dose. Quench correction for samples was not needed since counts were normalized to the dose and quenching did not vary from sample to sample.

In vitro AMPK activity measurement with total cell lysates

LNCaP95 cells were treated with BKIDC at 20 µM for 1 h. AMPK activity in total cell lysates was measured using CycLex AMPK Kinase Assay kit (MBL International Corporation) according to the manufacturer's instructions. Briefly, total cell lysates were prepared in lysis buffer (20 mM Tris-HCl, pH 7.5, 250 mM NaCl, 10% glycerol, 0.5% NP-40, 1 mM DTT) supplemented with Halt Protease Inhibitor Cocktail and Halt Phosphatase Cocktail (Thermo Fisher Scientific) and incubated for 30 min at 30°C in a pre-coated plate with an AMPK substrate peptide corresponding to mouse insulin receptor substrate-1 (IRS-1). AMPK activity was measured by monitoring the phosphorylation of Ser-789 in IRS-1 using an anti-mouse phospho-Ser-789 IRS-1 monoclonal antibody (with AS-4C4) and peroxidase-coupled anti-mouse IgG antibody.

Conversion of the chromogenic substrate tetramethylbenzidine was quantified by absorbance measurement at 450 nm.

Real-time cellular bioenergetic assay

We used Seahorse Bioscience XFe24 analyzer to measure extracellular acidification rate (ECAR) and oxygen consumption rate (OCR) which reflect the rates of glycolysis and oxidative phosphorylation, respectively. Cells were plated at 40,000 cells/well in Seahorse XF24 plates coated with 10 µg/ml PDL and incubated overnight. The culture medium was then replaced by Seahorse XF RPMI medium (Agilent: 103576-100) and cells were pre-incubated in a CO_2-free incubator at 37°C for 1 h prior to metabolic analysis. The effect of BKIDC was evaluated by pre-treating cells with 20 µM BKIDC during 1h-pre-incubation period with and without glucose prior to mitochondrial and glycolytic stress tests, respectively. Mitochondrial stress test was carried out by sequentially injecting oligomycin, FCCP, and rotenone/antimycin A. Glycolytic stress test was done by sequential injection of glucose, oligomycin, and 2-DG. The acute effect of SGI was assessed by directly adding BKIDC through the injection port. The bioenergetic profiles were analyzed from at least 3 biological replicates.

Measurement of intracellular ATP levels

50 K cells were plated on 48-plate and grown overnight. Cells were treated with the indicated compounds for 2 h unless specified. After removing culture media, 80 µL of the CellTiter Glo 2.0 assay kit (Promega) was added to the cells. After removing culture media, 80 µl of CellTiter-Glo Reagent was added to the cells. Intracellular ATP levels

under each condition were assessed on 96-well plate on GloMax® plate reader. The luminescence signal was proportional to the amount of ATP present in the solution.

CRISPR/Cas9-mediated genome editing.

We used a CRISPR/Cas9 approach to establish a stable knockout LNCaP cell lines deficient of either HK1 or HK2(*65*). sgRNA protospacer of HK1 (HK1-1: GGTGAGGTGGAAATGAGCCA; HK1-3: GGAGGGCAGCATCTTAACCA) and HK2 (HK2-1: GATGCGCCACATCGACATGG; HK2-2: TAAGCGGTTCCGCAAGGAGA) was cloned into lentiCRISPR v2 construct (Addgene 52961) using a protocol available online (Zhang_lab_LentiCRISPR_library_protocol.pdf). gRNA sequence (control: GTATTACTGATATTGGTGGG) was used to prepare the lentiviral construct for a non-targeting control(*66*). 293FT cells were seeded on 6-well plates coated with poly-D-lysine. The following day, 293T cells were co-transfected with lentiCRISPR v2 construct and the second-generation lentiviral packaging plasmids pMD2.G for VSV-G (Addgene 12259) and pCMVR8.74 for GAG, POL, TAT, and REV (Addgene 22036) using Lipofectamine 3000 reagent (Thermo Fisher Scientific). Lentivirus-containing supernatant was collected at 12 and 24 h after transfection, filtered through a 0.45-µm filter (Cytiva: WHA-9916-1304), and used to infect LNCaP as a recipient cell line, overnight in the presence of 5 µg/ml polybrene (Sigma, #107689). The infected cells were selected with 5 µg/ml of puromycin (ThermoFisher Scientific) for 3 days. Selected cells were immediately used as pool cell populations to evaluate glycolytic capacities in relation to BKIDC. On the other hand, to isolate morphologically single colonies, they were also plated at the density of 0.5 cell/well in 96-well plates in the conditioned media

from native LNCaP line. Resulting colonies were screened by Western blot analysis for loss of either HK1 or HK2 expression. After a second confirmatory Western blot analysis, the genomic junctions flanking corresponding sgRNA binding sites were amplified with sequence-specific primers by PCR using Platinum Taq DNA Polymerase and the amplicons were cloned into pCR™2.1-TOPO™ plasmid with TOPO™ TA Cloning™ Kit and Sanger-sequenced using the T7 promoter primmer and M13 Reverse primer. Particular isolates (HK11-9, HK13-5, HK21-5, HK22-1) were chosen for further experiments. Pool cell population which was infected with non-targeting control virus served as control cell lines for the experiments with both clonal cell lines and pool cell populations.

Cell proliferation assay

Cell proliferation was determined by MTS [3-(4,5-dimethylthiazol-2-yl)-5-(3-carboxymethoxyphenyl)-2-(4-sulfophenyl)-2H-tetrazolium, inner salt] assay using CellTiter 96® AQueous Non-Radioactive Cell Proliferation Assay (MTS) kit (Promega, Madison, WI) at 72 h after BKIDCs were added for all cell lines, except for VCaP at 120 h. Each cell line was tested in 96 well plates at 5000 cells/well in the culture media. The data shown are representative of at least two independent biological experiments, normalized to the values obtained from cells grown in medium containing 0.1% DMSO vehicle and presented as mean ± standard deviation (SD) (n=3-5).

Cell Cycle Analysis

Analysis was performed as previously described(*67*). Cells treated with BKIDCs for 30, 48, or 72 h were collected and resuspended in a solution of 10 µg/ml 4,6-diamidino-2-phenylindole (DAPI) and 0.1% Nonidet P-40 detergent in a Tris buffered saline. The suspension was analyzed on the LSR II flow cytometer (BD biosciences), with ultraviolet or violet excitation and DAPI emission collected at >450nm. DNA content and cell cycle are analyzed as previously described using the software program MultiCycle(*67*) (Phoenix Flow Systems, San Diego, CA).

Western blot analysis

Cells were lysed in M-Per lysis buffer (Thermo Fisher Scientific) supplemented with Halt Protease Inhibitor Cocktail and Halt Phosphatase Cocktail (ThermoFisher Scientific). Protein measurement was determined using the BCA assay (Pierce Biological). Samples were run on 4-15% SDS-PAGE gradient gels (Bio-Rad) and proteins transferred to PVDF membranes using TransBlot Turbo transfer system (Bio-Rad). Tris-buffered saline (TBS: 20 mM Tris-HCl, pH 7.5, containing 0.15 M NaCl) with 0.3% Tween 20 (TBS-T) was used. Membranes were blocked with the blocking buffer (TBS-T with 5% nonfat milk. Blots were incubated with appropriate antibodies in the blocking buffer (Detailed antibody information is provided in **Table S6**). TBS-T was used for all washes. Chemiluminescence and near-Infrared fluorescence imaging were performed with FluorChem R (ProteinSimple) and Odyssey® Imaging System (Li-COR Biosciences), respectively.

In vivo BKIDC-1553 studies

Male severe combined immunodeficient (SCID) mice were used for all in vivo experiments (Charles River Laboratories). PC3 (100,000 cells) were mixed 1:1 with Matrigel and injected subcutaneously into rear flanks of intact SCID mice (10 mice were enrolled per treatment group for PC3 study. When tumors reached ~100 mm^3, either vehicle (7% Tween-80, 3% EtOH in pharmaceutical grade PBS) or 20 mg/kg of BKIDC-1553 was given by oral gavage three times weekly (Mon, Wed, Fri), for up to 4 weeks. A patient-derived PCa xenograft, LuCaP 35, was implanted subcutaneously into rear flanks of intact SCID mice (The number of enrolled mice was: 8 for control, 9 for 1553, 7 for enzalutamide). When tumors reached ~100 mm^3, mice were given vehicle (7% Tween-80, 3% EtOH in pharmaceutical grade PBS), 20 mg/kg of BKIDC-1553, or 10 mg/kg enzalutamide by oral gavage three times weekly (Mon, Wed, Fri) for up to 5 weeks. All mice were assigned to treatment or control groups using a random number generator. ARRIVE guidelines were followed for all animal experiments. All animal studies were approved by the University of Washington Institutional Animal Care and Use Committee (protocol 2797-04).

Determining BKIDC-1553 concentrations in tumors

Each tumor was flushed with Dulbecco's phosphate-buffered saline (DPBS), weighed and placed in storage at -80°C. On the day of homogenization, 0.9% NaCl was added to each sample to achieve 100 mg/ml of tissue concentration. Samples were then homogenized using a handheld motorized homogenizer (Thermo Fisher Scientific) on ice, and 100 µL of each homogenate sample was placed in a 96-well plate. In addition,

tissues from vehicle control-treated mice were homogenized and placed in a 96-well plate to be used as blanks or standards. Calibration curves were generated individually for each type of tumor. An internal standard was added to each sample to a final concentration of 20 nM. All homogenates were stored at -80°C. On the day of tissue extraction, 10 µl of each sample were added to a 96-well plate that contained 90 µl of 80% ACN:20% water. The samples were mixed and centrifuged at 4,200 g for 20 min. 25 µL of the supernatants were placed in a 96-well plate that contained 475 µL of 80:20 ACN:water. Then, the samples were mixed and centrifuged at 4,200 g for 10 min. Supernatant from each sample was placed in a new 96-well plate, sealed and analyzed by LC-MS/MS. Sample concentrations were determined using the internal standard normalized calibration curves. To report tissue concentrations of BKIDC-1553, diluted homogenates were adjusted post-integration on a weight:weight basis. Individual tumor concentrations, means, and standard deviations are reported in Supplementary Table 5.

Statistical Analysis

Statistical analyses were conducted using GraphPad Prism v8 and are indicated within all figures. One-way ANOVA followed by Tukey's test for multiple comparison or 2-tailed unpaired t test was performed to determine significance, which was defined as $p < 0.05$.

List of Supplementary Materials

Supplementary Materials and Methods

Kinobead profiling of 1553-N-Me using a 1:1 mixture of HCT116/HEK293T lysate

Measurement of in vitro AMPK activity

Activity measurement of hexokinase

Synthesis of PP and PrP based BKIDCs

Figures S1 to S11

Tables S1 to S6

Uncropped Western blot images

References (68-71) incorporated into main reference section of paper

References

1. L. Wang, B. Lu, M. He, Y. Wang, Z. Wang, L. Du, Prostate Cancer Incidence and Mortality: Global Status and Temporal Trends in 89 Countries From 2000 to 2019. *Front Public Health* **10**, (2022).
2. R. J. Rebello, C. Oing, K. E. Knudsen, S. Loeb, D. C. Johnson, R. E. Reiter, S. Gillessen, T. Van der Kwast, R. G. Bristow, Prostate cancer. *Nat Rev Dis Primers* **7**, 9 (2021).
3. S. Sumanasuriya, J. De Bono, Treatment of Advanced Prostate Cancer-A Review of Current Therapies and Future Promise. *Cold Spring Harb Perspect Med* **8**, (2018).
4. P. A. Watson, V. K. Arora, C. L. Sawyers, Emerging mechanisms of resistance to androgen receptor inhibitors in prostate cancer. *Nat Rev Cancer* **15**, 701-711 (2015).
5. J. Mateo, C. J. Lord, V. Serra, A. Tutt, J. Balmana, M. Castroviejo-Bermejo, C. Cruz, A. Oaknin, S. B. Kaye, J. S. de Bono, A decade of clinical development of PARP inhibitors in perspective. *Ann Oncol* **30**, 1437-1447 (2019).
6. O. Sartor, J. de Bono, K. N. Chi, K. Fizazi, K. Herrmann, K. Rahbar, S. T. Tagawa, L. T. Nordquist, N. Vaishampayan, G. El-Haddad, C. H. Park, T. M. Beer, A. Armour, W. J. Perez-Contreras, M. DeSilvio, E. Kpamegan, G. Gericke, R. A. Messmann, M. J. Morris, B. J. Krause, V. Investigators, Lutetium-177-PSMA-617 for Metastatic Castration-Resistant Prostate Cancer. *N Engl J Med* **385**, 1091-1103 (2021).
7. C. Parker, S. Nilsson, D. Heinrich, S. I. Helle, J. M. O'Sullivan, S. D. Fossa, A. Chodacki, P. Wiechno, J. Logue, M. Seke, A. Widmark, D. C. Johannessen, P. Hoskin, D. Bottomley, N. D. James, A. Solberg, I. Syndikus, J. Kliment, S. Wedel, S. Boehmer, M. Dall'Oglio, L. Franzen, R. Coleman, N. J. Vogelzang, C. G. O'Bryan-Tear, K. Staudacher, J. Garcia-Vargas, M. Shan, O. S. Bruland, O. Sartor, A. Investigators, Alpha emitter radium-223 and survival in metastatic prostate cancer. *N Engl J Med* **369**, 213-223 (2013).
8. J. Mateo, R. McKay, W. Abida, R. Aggarwal, J. Alumkal, A. Alva, F. Feng, X. Gao, J. Graff, M. Hussain, F. Karzai, B. Montgomery, W. Oh, V. Patel, D. Rathkopf, M. Rettig, N. Schultz, M. Smith, D. Solit, C. Sternberg, E. Van Allen, D. VanderWeele, J. Vinson, H. R. Soule, A. Chinnaiyan, E. Small, J. W. Simons, W. Dahut, A. K. Miyahira, H. Beltran, Accelerating precision medicine in metastatic prostate cancer. *Nat Cancer* **1**, 1041-1053 (2020).
9. S. Y. C. Choi, C. F. Ribeiro, Y. Wang, M. Loda, S. R. Plymate, T. Uo, Druggable Metabolic Vulnerabilities Are Exposed and Masked during Progression to Castration Resistant Prostate Cancer. *Biomolecules* **12**, (2022).
10. G. Zadra, C. F. Ribeiro, P. Chetta, Y. Ho, S. Cacciatore, X. Gao, S. Syamala, C. Bango, C. Photopoulos, Y. Huang, S. Tyekucheva, D. C. Bastos, J. Tchaicha, B. Lawney, T. Uo, L. D'Anello, A. Csibi, R. Kalekar, B. Larimer, L. Ellis, L. M. Butler, C. Morrissey, K. McGovern, V. J. Palombella, J. L. Kutok, U. Mahmood, S. Bosari, J. Adams, S. Peluso, S. M. Dehm, S. R. Plymate, M. Loda, Inhibition of de novo lipogenesis targets androgen receptor signaling in castration-resistant prostate cancer. *Proc Natl Acad Sci U S A* **116**, 631-640 (2019).
11. X. Zhang, C. V. Dang, Time to hit pause on mitochondria-targeting cancer therapies. *Nat Med* **29**, 29-30 (2023).
12. D. Hanahan, R. A. Weinberg, Hallmarks of cancer: the next generation. *Cell* **144**, 646-674 (2011).
13. B. Faubert, A. Solmonson, R. J. DeBerardinis, Metabolic reprogramming and cancer progression. *Science* **368**, (2020).
14. M. G. Vander Heiden, R. J. DeBerardinis, Understanding the Intersections between Metabolism and Cancer Biology. *Cell* **168**, 657-669 (2017).

15. Z. E. Stine, Z. T. Schug, J. M. Salvino, C. V. Dang, Targeting cancer metabolism in the era of precision oncology. *Nat Rev Drug Discov* **21**, 141-162 (2022).
16. O. Warburg, Über den Stoffwechsel der Carcinomzelle. *Naturwissenschaften* **12**, 1131-1137 (1924).
17. B. R. Landau, J. Laszlo, J. Stengle, D. Burk, Certain metabolic and pharmacologic effects in cancer patients given infusions of 2-deoxy-D-glucose. *J Natl Cancer Inst* **21**, 485-494 (1958).
18. F. Ahmad, M. K. Cherukuri, P. L. Choyke, Metabolic reprogramming in prostate cancer. *Br J Cancer* **125**, 1185-1196 (2021).
19. T. Uo, C. C. Sprenger, S. R. Plymate, Androgen Receptor Signaling and Metabolic and Cellular Plasticity During Progression to Castration Resistant Prostate Cancer. *Front Oncol* **10**, 580617 (2020).
20. S. Cameron, G. Deblois, J. R. Hawley, A. Qamra, S. Zhou, S. A. M. Tonekaboni, A. Murison, R. Van Vliet, J. Liu, J. W. Locasale, M. Lupien, Chronic hypoxia favours adoption to a castration-resistant cell state in prostate cancer. *Oncogene* **42**, 1693-1703 (2023).
21. A. K. Beier, M. Puhr, M. B. Stope, C. Thomas, H. H. H. Erb, Metabolic changes during prostate cancer development and progression. *J Cancer Res Clin Oncol* **149**, 2259-2270 (2023).
22. K. C. Patra, Q. Wang, P. T. Bhaskar, L. Miller, Z. Wang, W. Wheaton, N. Chandel, M. Laakso, W. J. Muller, E. L. Allen, A. K. Jha, G. A. Smolen, M. F. Clasquin, B. Robey, N. Hay, Hexokinase 2 is required for tumor initiation and maintenance and its systemic deletion is therapeutic in mouse models of cancer. *Cancer Cell* **24**, 213-228 (2013).
23. S. M. Davidson, D. R. Schmidt, J. E. Heyman, J. P. O'Brien, A. C. Liu, W. J. Israelsen, T. L. Dayton, R. Sehgal, R. T. Bronson, E. Freinkman, H. H. Mak, G. N. Fanelli, S. Malstrom, G. Bellinger, A. Carracedo, P. P. Pandolfi, K. D. Courtney, A. Jha, R. A. DePinho, J. W. Horner, C. J. Thomas, L. C. Cantley, M. Loda, M. G. Vander Heiden, Pyruvate Kinase M1 Suppresses Development and Progression of Prostate Adenocarcinoma. *Cancer Res* **82**, 2403-2416 (2022).
24. L. Wang, H. Xiong, F. Wu, Y. Zhang, J. Wang, L. Zhao, X. Guo, L. J. Chang, Y. Zhang, M. J. You, S. Koochekpour, M. Saleem, H. Huang, J. Lu, Y. Deng, Hexokinase 2-mediated Warburg effect is required for PTEN- and p53-deficiency-driven prostate cancer growth. *Cell Rep* **8**, 1461-1474 (2014).
25. M. Golkowski, R. S. Vidadala, C. K. Lombard, H. W. Suh, D. J. Maly, S. E. Ong, Kinobead and Single-Shot LC-MS Profiling Identifies Selective PKD Inhibitors. *J Proteome Res* **16**, 1216-1227 (2017).
26. M. Tandon, J. M. Salamoun, E. J. Carder, E. Farber, S. Xu, F. Deng, H. Tang, P. Wipf, Q. J. Wang, SD-208, a novel protein kinase D inhibitor, blocks prostate cancer cell proliferation and tumor growth in vivo by inducing G2/M cell cycle arrest. *PLoS One* **10**, e0119346 (2015).
27. Tandon M, Johnson J, Li Z, Xu S, Wipf P, W. QJ, New pyrazolopyrimidine inhibitors of protein kinase D as potent anticancer agents for prostate cancer cells. *PloS ONE* **8**, e75601 (2013).
28. R. S. Vidadala, K. L. Rivas, K. K. Ojo, M. A. Hulverson, J. A. Zambriski, I. Bruzual, T. L. Schultz, W. Huang, Z. Zhang, S. Scheele, A. E. DeRocher, R. Choi, L. K. Barrett, L. K. Siddaramaiah, W. G. Hol, E. Fan, E. A. Merritt, M. Parsons, G. Freiberg, K. Marsh, D. J. Kempf, V. B. Carruthers, N. Isoherranen, J. S. Doggett, W. C. Van Voorhis, D. J. Maly, Development of an Orally Available and Central Nervous System (CNS) Penetrant Toxoplasma gondii Calcium-Dependent Protein Kinase 1 (TgCDPK1) Inhibitor with Minimal Human Ether-a-go-go-Related Gene (hERG) Activity for the Treatment of Toxoplasmosis. *J Med Chem* **59**, 6531-6546 (2016).

29. E. G. Bluemn, I. M. Coleman, J. M. Lucas, R. T. Coleman, S. Hernandez-Lopez, R. Tharakan, D. Bianchi-Frias, R. F. Dumpit, A. Kaipainen, A. N. Corella, Y. C. Yang, M. D. Nyquist, E. Mostaghel, A. C. Hsieh, X. Zhang, E. Corey, L. G. Brown, H. M. Nguyen, K. Pienta, M. Ittmann, M. Schweizer, L. D. True, D. Wise, P. S. Rennie, R. L. Vessella, C. Morrissey, P. S. Nelson, Androgen Receptor Pathway-Independent Prostate Cancer Is Sustained through FGF Signaling. *Cancer Cell* **32**, 474-489.e476 (2017).
30. A. Shrestha, K. K. Ojo, F. Koston, B. Ruttkowski, R. S. R. Vidadala, C. S. Dorr, E. D. Navaluna, G. R. Whitman, K. F. Barrett, L. K. Barrett, M. A. Hulverson, R. Choi, S. A. Michaels, D. J. Maly, A. Hemphill, W. C. Van Voorhis, A. Joachim, Bumped kinase inhibitor 1369 is effective against Cystoisospora suis in vivo and in vitro. *Int J Parasitol Drugs Drug Resist* **10**, 9-19 (2019).
31. D. Wlodkowic, W. Telford, J. Skommer, Z. Darzynkiewicz, Apoptosis and beyond: cytometry in studies of programmed cell death. *Methods Cell Biol* **103**, 55-98 (2011).
32. T. S. Gujral, R. L. Karp, A. Finski, M. Chan, P. E. Schwartz, G. MacBeath, P. Sorger, Profiling phospho-signaling networks in breast cancer using reverse-phase protein arrays. *Oncogene* **32**, 3470-3476 (2013).
33. D. Garcia, R. J. Shaw, AMPK: Mechanisms of Cellular Energy Sensing and Restoration of Metabolic Balance. *Mol Cell* **66**, 789-800 (2017).
34. O. Meyuhas, Ribosomal Protein S6 Phosphorylation: Four Decades of Research. *Int Rev Cell Mol Biol* **320**, 41-73 (2015).
35. B. Cool, B. Zinker, W. Chiou, L. Kifle, N. Cao, M. Perham, R. Dickinson, A. Adler, G. Gagne, R. Iyengar, G. Zhao, K. Marsh, P. Kym, P. Jung, H. S. Camp, E. Frevert, Identification and characterization of a small molecule AMPK activator that treats key components of type 2 diabetes and the metabolic syndrome. *Cell Metab* **3**, 403-416 (2006).
36. N. D. C. M. Lehninger AL, Principles of Biochemistry, 2nd edn. *textbook*, (1993).
37. S. A. Mookerjee, D. G. Nicholls, M. D. Brand, Determining Maximum Glycolytic Capacity Using Extracellular Flux Measurements. *PLoS One* **11**, e0152016 (2016).
38. A. A. Gerencser, A. Neilson, S. W. Choi, U. Edman, N. Yadava, R. J. Oh, D. A. Ferrick, D. G. Nicholls, M. D. Brand, Quantitative microplate-based respirometry with correction for oxygen diffusion. *Analytical chemistry* **81**, 6868-6878 (2009).
39. M. R. Antoniewicz, A guide to (13)C metabolic flux analysis for the cancer biologist. *Exp Mol Med* **50**, 19 (2018).
40. J. F. Tanti, M. Cormont, T. Gremeaux, Y. Le Marchand-Brustel, Assays of glucose entry, glucose transporter amount, and translocation. *Methods in molecular biology (Clifton, N.J.)* **155**, 157-165 (2001).
41. Z. Farooq, H. Ismail, S. A. Bhat, B. T. Layden, M. W. Khan, Aiding Cancer's "Sweet Tooth": Role of Hexokinases in Metabolic Reprogramming. *Life (Basel)* **13**, (2023).
42. M. Ghandi, F. W. Huang, J. Jane-Valbuena, G. V. Kryukov, C. C. Lo, E. R. McDonald, 3rd, J. Barretina, E. T. Gelfand, C. M. Bielski, H. Li, K. Hu, A. Y. Andreev-Drakhlin, J. Kim, J. M. Hess, B. J. Haas, F. Aguet, B. A. Weir, M. V. Rothberg, B. R. Paolella, M. S. Lawrence, R. Akbani, Y. Lu, H. L. Tiv, P. C. Gokhale, A. de Weck, A. A. Mansour, C. Oh, J. Shih, K. Hadi, Y. Rosen, J. Bistline, K. Venkatesan, A. Reddy, D. Sonkin, M. Liu, J. Lehar, J. M. Korn, D. A. Porter, M. D. Jones, J. Golji, G. Caponigro, J. E. Taylor, C. M. Dunning, A. L. Creech, A. C. Warren, J. M. McFarland, M. Zamanighomi, A. Kauffmann, N. Stransky, M. Imielinski, Y. E. Maruvka, A. D. Cherniack, A. Tsherniak, F. Vazquez, J. D. Jaffe, A. A. Lane, D. M. Weinstock, C. M. Johannessen, M. P. Morrissey, F. Stegmeier, R. Schlegel, W. C. Hahn, G. Getz, G. B. Mills, J. S. Boehm, T. R. Golub, L. A. Garraway, W. R. Sellers, Next-generation characterization of the Cancer Cell Line Encyclopedia. *Nature* **569**, 503-508 (2019).

43. E. Corey, J. E. Quinn, K. R. Buhler, P. S. Nelson, J. A. Macoska, L. D. True, R. L. Vessella, LuCaP 35: a new model of prostate cancer progression to androgen independence. *Prostate* **55**, 239-246 (2003).
44. P. Chetta, G. Zadra, Metabolic reprogramming as an emerging mechanism of resistance to endocrine therapies in prostate cancer. *Cancer Drug Resist* **4**, 143-162 (2021).
45. J. J. Fox, S. C. Gavane, E. Blanc-Autran, S. Nehmeh, M. Gonen, B. Beattie, H. A. Vargas, H. Schoder, J. L. Humm, S. W. Fine, J. S. Lewis, S. B. Solomon, J. R. Osborne, D. Veach, C. L. Sawyers, W. A. Weber, H. I. Scher, M. J. Morris, S. M. Larson, Positron Emission Tomography/Computed Tomography-Based Assessments of Androgen Receptor Expression and Glycolytic Activity as a Prognostic Biomarker for Metastatic Castration-Resistant Prostate Cancer. *JAMA Oncol* **4**, 217-224 (2018).
46. H. Jadvar, Is There Use for FDG-PET in Prostate Cancer? *Semin Nucl Med* **46**, 502-506 (2016).
47. M. K. Bakht, J. M. Lovnicki, J. Tubman, K. F. Stringer, J. Chiaramonte, M. R. Reynolds, I. Derecichei, R. M. Ferraiuolo, B. A. Fifield, D. Lubanska, S. W. Oh, G. J. Cheon, C. Kwak, C. W. Jeong, K. W. Kang, J. F. Trant, C. Morrissey, I. M. Coleman, Y. Wang, H. Ahmadzadehfar, X. Dong, L. A. Porter, Differential Expression of Glucose Transporters and Hexokinases in Prostate Cancer with a Neuroendocrine Gene Signature: A Mechanistic Perspective for (18)F-FDG Imaging of PSMA-Suppressed Tumors. *J Nucl Med* **61**, 904-910 (2020).
48. A. G. Wibmer, M. J. Morris, M. Gonen, J. Zheng, H. Hricak, S. Larson, H. I. Scher, H. A. Vargas, Quantification of Metastatic Prostate Cancer Whole-Body Tumor Burden with (18)F-FDG PET Parameters and Associations with Overall Survival After First-Line Abiraterone or Enzalutamide: A Single-Center Retrospective Cohort Study. *J Nucl Med* **62**, 1050-1056 (2021).
49. W. Shan, Y. Zhou, K. Y. Tam, The development of small-molecule inhibitors targeting hexokinase 2. *Drug Discov Today* **27**, 2574-2585 (2022).
50. F. Ciscato, R. Filadi, I. Masgras, M. Pizzi, O. Marin, N. Damiano, P. Pizzo, A. Gori, F. Frezzato, F. Chiara, L. Trentin, P. Bernardi, A. Rasola, Hexokinase 2 displacement from mitochondria-associated membranes prompts Ca(2+) -dependent death of cancer cells. *EMBO Rep* **21**, e49117 (2020).
51. W. Shan, Y. Zhou, K. Y. Tam, The development of small-molecule inhibitors targeting hexokinase 2. *Drug Discov Today*, (2022).
52. F. Ciscato, L. Ferrone, I. Masgras, C. Laquatra, A. Rasola, Hexokinase 2 in Cancer: A Prima Donna Playing Multiple Characters. *Int J Mol Sci* **22**, (2021).
53. S. Xu, H. R. Herschman, A Tumor Agnostic Therapeutic Strategy for Hexokinase 1-Null/Hexokinase 2-Positive Cancers. *Cancer Res* **79**, 5907-5914 (2019).
54. J. Barretina, G. Caponigro, N. Stransky, K. Venkatesan, A. A. Margolin, S. Kim, C. J. Wilson, J. Lehar, G. V. Kryukov, D. Sonkin, A. Reddy, M. Liu, L. Murray, M. F. Berger, J. E. Monahan, P. Morais, J. Meltzer, A. Korejwa, J. Jane-Valbuena, F. A. Mapa, J. Thibault, E. Bric-Furlong, P. Raman, A. Shipway, I. H. Engels, J. Cheng, G. K. Yu, J. Yu, P. Aspesi, Jr., M. de Silva, K. Jagtap, M. D. Jones, L. Wang, C. Hatton, E. Palescandolo, S. Gupta, S. Mahan, C. Sougnez, R. C. Onofrio, T. Liefeld, L. MacConaill, W. Winckler, M. Reich, N. Li, J. P. Mesirov, S. B. Gabriel, G. Getz, K. Ardlie, V. Chan, V. E. Myer, B. L. Weber, J. Porter, M. Warmuth, P. Finan, J. L. Harris, M. Meyerson, T. R. Golub, M. P. Morrissey, W. R. Sellers, R. Schlegel, L. A. Garraway, The Cancer Cell Line Encyclopedia enables predictive modelling of anticancer drug sensitivity. *Nature* **483**, 603-607 (2012).
55. V. Nogueira, K. C. Patra, N. Hay, Selective eradication of cancer displaying hyperactive Akt by exploiting the metabolic consequences of Akt activation. *Elife* **7**, (2018).

56. S. Xu, A. Catapang, D. Braas, L. Stiles, H. M. Doh, J. T. Lee, T. G. Graeber, R. Damoiseaux, O. Shirihai, H. R. Herschman, A precision therapeutic strategy for hexokinase 1-null, hexokinase 2-positive cancers. *Cancer Metab* **6**, 7 (2018).
57. H. Beltran, A. Hruszkewycz, H. I. Scher, J. Hildesheim, J. Isaacs, E. Y. Yu, K. Kelly, D. Lin, A. Dicker, J. Arnold, T. Hecht, M. Wicha, R. Sears, D. Rowley, R. White, J. L. Gulley, J. Lee, M. Diaz Meco, E. J. Small, M. Shen, K. Knudsen, D. W. Goodrich, T. Lotan, A. Zoubeidi, C. L. Sawyers, C. M. Rudin, M. Loda, T. Thompson, M. A. Rubin, A. Tawab-Amiri, W. Dahut, P. S. Nelson, The Role of Lineage Plasticity in Prostate Cancer Therapy Resistance. *Clin Cancer Res* **25**, 6916-6924 (2019).
58. A. H. Davies, H. Beltran, A. Zoubeidi, Cellular plasticity and the neuroendocrine phenotype in prostate cancer. *Nat Rev Urol* **15**, 271-286 (2018).
59. D. Vara-Ciruelos, M. Dandapani, D. G. Hardie, AMP-Activated Protein Kinase: Friend or Foe in Cancer? *Annual Review of Cancer Biology* **4**, 1-16 (2020).
60. D. DeWaal, V. Nogueira, A. R. Terry, K. C. Patra, S.-M. Jeon, G. Guzman, J. Au, C. P. Long, M. R. Antoniewicz, N. Hay, Hexokinase-2 depletion inhibits glycolysis and induces oxidative phosphorylation in hepatocellular carcinoma and sensitizes to metformin. *Nature Communications* **9**, 446 (2018).
61. A. Mendez-Lucas, W. Lin, P. C. Driscoll, N. Legrave, L. Novellasdemunt, C. Xie, M. Charles, Z. Wilson, N. P. Jones, S. Rayport, M. Rodriguez-Justo, V. Li, J. I. MacRae, N. Hay, X. Chen, M. Yuneva, Identifying strategies to target the metabolic flexibility of tumours. *Nat Metab* **2**, 335-350 (2020).
62. W. Guo, Y. Kuang, J. Wu, D. Wen, A. Zhou, Y. Liao, H. Song, D. Xu, T. Wang, B. Jing, K. Li, M. Hu, J. Ling, Q. Wang, W. Wu, Hexokinase 2 Depletion Confers Sensitization to Metformin and Inhibits Glycolysis in Lung Squamous Cell Carcinoma. *Front Oncol* **10**, 52 (2020).
63. D. Gao, I. Vela, A. Sboner, P. J. Iaquinta, W. R. Karthaus, A. Gopalan, C. Dowling, J. N. Wanjala, E. A. Undvall, V. K. Arora, J. Wongvipat, M. Kossai, S. Ramazanoglu, L. P. Barboza, W. Di, Z. Cao, Q. F. Zhang, I. Sirota, L. Ran, T. Y. MacDonald, H. Beltran, J. M. Mosquera, K. A. Touijer, P. T. Scardino, V. P. Laudone, K. R. Curtis, D. E. Rathkopf, M. J. Morris, D. C. Danila, S. F. Slovin, S. B. Solomon, J. A. Eastham, P. Chi, B. Carver, M. A. Rubin, H. I. Scher, H. Clevers, C. L. Sawyers, Y. Chen, Organoid cultures derived from patients with advanced prostate cancer. *Cell* **159**, 176-187 (2014).
64. I. R. Sweet, D. L. Cook, A. Lernmark, C. J. Greenbaum, A. R. Wallen, E. S. Marcum, S. A. Stekhova, K. A. Krohn, Systematic screening of potential beta-cell imaging agents. *Biochem Biophys Res Commun* **314**, 976-983 (2004).
65. N. E. Sanjana, O. Shalem, F. Zhang, Improved vectors and genome-wide libraries for CRISPR screening. *Nat Methods* **11**, 783-784 (2014).
66. J. G. Doench, N. Fusi, M. Sullender, M. Hegde, E. W. Vaimberg, K. F. Donovan, I. Smith, Z. Tothova, C. Wilen, R. Orchard, H. W. Virgin, J. Listgarten, D. E. Root, Optimized sgRNA design to maximize activity and minimize off-target effects of CRISPR-Cas9. *Nat Biotechnol* **34**, 184-191 (2016).
67. P. S. Rabinovitch, DNA content histogram and cell-cycle analysis. *Methods Cell Biol* **41**, 263-296 (1994).
68. R. Choi, A. Kelley, D. Leibly, S. N. Hewitt, A. Napuli, W. Van Voorhis, Immobilized metal-affinity chromatography protein-recovery screening is predictive of crystallographic structure success. *Acta Crystallogr Sect F Struct Biol Cryst Commun* **67**, 998-1005 (2011).
69. K. K. Ojo, J. R. Gillespie, A. J. Riechers, A. J. Napuli, C. L. Verlinde, F. S. Buckner, M. H. Gelb, M. M. Domostoj, S. J. Wells, A. Scheer, T. N. Wells, W. C. Van Voorhis, Glycogen synthase kinase 3 is a potential drug target for African trypanosomiasis therapy. *Antimicrob Agents Chemother* **52**, 3710-3717 (2008).

70. F. W. Studier, Protein production by auto-induction in high density shaking cultures. *Protein Expr Purif* **41**, 207-234 (2005).
71. K. F. Barrett, D. M. Dranow, I. Q. Phan, S. A. Michaels, S. Shaheen, E. D. Navaluna, J. K. Craig, L. M. Tillery, R. Choi, T. E. Edwards, D. G. Conrady, J. Abendroth, P. S. Horanyi, D. D. Lorimer, W. C. Van Voorhis, Z. Zhang, L. K. Barrett, S. Subramanian, B. Staker, E. Fan, P. J. Myler, O. O. Soge, K. Hybiske, K. K. Ojo, Structures of glyceraldehyde 3-phosphate dehydrogenase in Neisseria gonorrhoeae and Chlamydia trachomatis. *Protein Sci* **29**, 768-778 (2020).

Acknowledgements:

We thank Dr. Taran Gujral and Stella Shin (Fred Hutchinson Cancer Center) for help with the RPPA data, Michael S. Dey PhD and D. Bruce Burlington PhD for their consultation, Dr. Michael Schweizer for discussion and manuscript editing, and Mika Munari for technical assistance.

Funding:

Lopker Family Foundation in honor of Karl Lopker, who died of prostate cancer in 2018

WE-REACH, supported by University of Washington and National Institutes of Health grant 5U01HL152401

US Department of Defense grant W81XWH-17-1-0323 (SRP, DM, WCVV)

US Department of Defense grant W81XWH-20-1-0146, (SRP)

US Department of Veterans Affairs Merit Review grant I01BX0033248 (SRP)

US Department of Veterans Affairs Service Directed Project number SDR-PLYMATE (SRP)

National Institutes of Health/National Cancer Institute grant CA255830 (TU) and National Institutes of Health/National Cancer Institute grant P50CA097186 (KKO).

Author contributions:

Conceptualization: TU, SRP, WCVV

Methodology: TU, DMJ, SRP

Investigation: TU, SRP, KKO, CCS, KSE, BGKP, MD, SS, SK, HHH, MAH, RC, GKP, GRW, SAM, LHX, HJP, MMN, ALBGV, VK, LBS, IRS, RV

Visualization: TU, KKO, CCS, KSE, BGKP, MD, SRP

Funding acquisition: TU, KKO, DMJ, SRP, WCVV

Project administration: SRP, LKB, WCVV

Supervision: LBS, IRS, DMJ, SRP, WCVV

Writing – original draft: TU, KKO, SRP, WCVV,

Writing – review & editing: TU, CCS, KKO, DMJ, GKP, SRP, WCVV, RC, MAH

Competing interests:

SRP is the President, WCVV is the Chief Executive Officer, DJM is the Chief Scientific Officer, and KKO is the Secretary of ProsTech Inc. ProsTech Inc. was created to commercialize therapies for prostate cancer, but as yet, has no commercial claims on BKIDCs or any other potential commercial products. Other authors declare that they have no competing interests.

Data and materials availability:

All data are available in the main text or the supplementary materials. All cell lines and plasmids generated in this study will be made available upon request from the lead contacts without restriction. Further information and requests for

resources and reagents should be directed to and will be fulfilled by lead contacts Stephen Plymate (splymate@uw.edu), Wesley Van Voorhis (wesley@uw.edu), and Takuma Uo (tuo@uw.edu).

Figure 1. BKIDC effects on Prostate Cancer Cell lines and other Cell Lines.

(A) Cell proliferation was evaluated by MTS assay at 72 h after BKIDC-1553 was added at the range between 0.63-20 μM, except for VCaP at 120 h (DMSO as a vehicle control). The data shown are representative of at least two independent experiments, normalized to the values obtained from cells grown in medium containing 0.1% DMSO vehicle and presented as mean ± standard deviation (SD) (n=3-5). One-way ANOVA followed by Tukey's test for multiple comparison: $^{**}p < 0.01$. **(B)** Structures of representative BKIDCs. Lead BKIDCs have two main scaffolds: Pyrrolopyrimidines (PrP) and pyrazolopyrimidines (PP) are two main scaffolds of BKIDCs. *Toxoplasma gondii* calcium dependent protein kinase 1 (*Tg*CDPK1) has the small gatekeeper residue glycine and can hold BKIDC-1553 in the ATP binding pocket. BKIDC-1553-N-Me, 1820, and GP228 have distinct R2 groups while commonly lacking the protein kinase binding and thus inhibition activity. **(C)** Graphical presentation of screening results of over 123 BKIDC compounds (**Table S1**) tested at 10 μM in LNCaP95 and PC3 (**Table S2**). Each dot represents one compound and the data are shown as mean ± SD. Compounds were categorized into three groups depending on the degree of inhibition of proliferation in LNCaP95 and PC3.

Figure 2. Cytostatic effects of anti-proliferative BKIDCs. (A) The percentage of cells at G1, S, and G2 phase of cell cycle at 30 h after treatment with the indicated BKIDCs. Cell cycle analysis showing G1 cell cycle arrest in LNCaP and LNCaP95 cells compared to PC3 when treated with BKIDC-1553 and 1553-N-Me. **(B)** Heat map of antigen levels detected by RPPA. Cellular lysates of LNCaP95 treated with the

indicated BKIDC at 20 μM for 24 h were subjected to RPPA with 70 distinct antibodies (Antibodies and the corresponding RPPA signal intensities relative to β-actin signals are listed in **Table S3**). Note BKIDC-1553 and 1553-N-Me commonly affected only abundance of ribosomal S6 protein (RPS6) phosphorylated at S235/S236 or S240/S244, the first two bands seen with BKIDC-1553 and the only bands seen with BKIDC-1553-N-Me. The response to BKIDC-1817 was comparable to the one to DMSO. **(C)** Time course and dose dependent studies of BKIDCs in LNCaP95 and PC3. Time- and dose-dependent decrease in phosphorylated RPS6 signals in RPPA in LNCaP95 but not PC3 as early as at 4 h after treatment with BKIDC-1553 and 1553-N-Me.

Figure 3. BKIDCs display 2-DG like activities. (A) AMPK activation in LNCaP95 treated with BKIDC-1553-N-Me. AMPK activity in total LNCaP95 lysates was measured after 1 h exposure to BKIDC-1553-N-Me or 1817. One-way ANOVA followed by Tukey's test for multiple comparison: $^{**}p < 0.01$. **(B)** Phosphorylated acetyl-CoA carboxylase (P-ACC) at Ser79 was increased after treatment with BKIDC-1553 but not 1817. Metabolic inhibitors 2-deoxyglucose (2-DG) and oligomycin (oligo) served as positive controls for AMPK activation to increase P-ACC. **(C)** Effects of BKIDCs on intracellular ATP levels in LNCaP and LNCaP95 cells. Cells were treated with BKIDC-1553-N-Me, glycolysis inhibitor 2-DG, and OXPHOS inhibitors (OXPHOSi) singly or in combination for 120 min. The data shown are representative of at least two independent experiments, normalized to the values obtained from cells grown in medium containing 0.1% DMSO vehicle and presented as mean ± SD (n=2). Rot: rotenone, FCCP: carbonyl cyanite-4

(trifluoromethoxy) phenylhydrazone, AA: Antimycin A. **(D)** LNCaP cells were treated with BKIDCs, 2-DG, and oligomycin (Oligo) singly or in combination for 8 and 24 h. BKIDCs and 2-DG cooperated with Oligo to promote cleavage of PARP at 24 h but not 8 h-treatment in LNCaP. This biochemical event was reflected by appearances of detached cells in the phase-contrast microscopic images.

Figure 4. Effect of BKIDC on glycolysis. (A) Extracellular acidification rates (ECAR) were determined in cultured cells by the Seahorse XFe24 analyzer. Cells were pre-treated with 20 μM BKIDC for 1 h prior to application to Seahorse analyzer. Increase in ECAR by glucose injection (glycolytic rates) was inhibited by BKIDC-1553-N-Me in LNCaP95 but not PC3. Maximum glycolytic capacity was evaluated by oligomycin injection. 2-DG injection shuts down glycolysis as reflected by return of ECAR to the basal levels. **(B)** The effect of BKIDC-1553-N-Me on glycolytic rates. The data shown are normalized to the values obtained from cells pre-treated with DMSO vehicle and presented as mean ± SD (n=3). One-way ANOVA followed by Tukey's test for multiple comparison: $^{**}p < 0.01$. **(C)** Cells were exposed to BKIDC at the indicated time by injection at the final concentration of 10 μM. Decrease in ECAR was observed in LNCaP95 but not PC3 immediately after injection of BKIDC-1553-N-Me. There was a compensatory increase in oxygen consumption rates (OCR) which reflects mitochondrial oxidative respiration.

Figure 5. Metabolic flux assay with ^{13}C-labeled glucose with BKIDC-1553-N-Me. **(A)** Schematic flowchart of glycolysis and the metabolites measured in this experiment (dark boxes). **(B)** Metabolic flux assay with ^{13}C-labeled glucose. ^{13}C enrichment of glycolytic intermediates was determined by liquid chromatography coupled with mass spectrometry (LC-MS) in DU145, LNCaP, and LNCaP95 cells at 30 min after exposure to [U-^{13}C]-glucose in the presence and absence of BKIDC-1553-N-Me. The X-axis is the concentration of BKIDC-1553-N-Me, with 0-20 μM added to the indicated cell lines. Black columns indicate where unlabeled carbon (^{12}C, thus M+0 [M=mass expected for ^{12}C]) is found and grey columns originate from the ^{13}C-labeled glucose (^{13}C, thus M+6 or M+3). In LNCaP and LNCaP95 cells, addition of BKIDC-1553-N-Me inhibited glucose being metabolized to 3-carbon glycolytic intermediates, DHAP, PG, PEP, or pyruvate, indicating a block in glycolysis, at or prior to the six-carbon to 3-carbon fructose-bisphosphate aldolase step. Note that in BKIDC non-responsive DU145 cells there is no BKIDC-1553-N-Me effect on hexose-6-phosphate and 3-carbon glycolytic intermediates (DHAP, PEP, PG, or pyruvate). The results trended to indicate that BKIDC blocked effects at hexose-6-phosphate levels. One-way ANOVA followed by Tukey's test for multiple comparison for M +3 and M + 6 isotopomers: *p <0.05, **p <0.01, ***p <0.001, ****p <0.0001.

Figure 6. Radiometric glucose uptake assay with radiolabeled glucose analogs in LNCaP and DU145 cells. (A) To distinguish between glucose uptake and phosphorylation steps, two different radiolabeled glucose analogs were used for radiometric assays. Both 2-DG and 3-O-methylglucose (3-OMG) are taken up into cells in the same manner as glucose. Unlike 2-DG which is trapped by hexokinase (HK)-mediated phosphorylation and accumulated in the cells as a form of 2-DG-6P, 3-OMG is not phosphorylated, and its intracellular levels reflect the cells' capability of Glut1-mediated glucose uptake itself. **(B)** 2-DG 2-[1,2-^{3}H(N)] accumulation was inhibited by the presence of BKIDC-1553-N-Me at 20 μM in LNCaP but not DU145 cell lines. 3-O-[methyl-^{3}H] D-glucose uptake was not affected by BKIDC-1553-N-Me in LNCaP. These data support the conclusion that BKIDC block phosphorylation but not uptake of glucose in BKIDC-susceptible cell line LNCaP cell line. One-way ANOVA followed by Tukey's test for multiple comparison: ****p <0.0001

Figure 7. The effect of HK deficiency on anti-glycolytic actions of BKIDC-1553-N-Me. (A) CRISPR-Cas9 system was used to generate HK1 and HK2 knock-out (KO) LNCaP clones and two independently derived KO clones for HK1 and HK2 were tested. Intracellular ATP levels, in the presence of a mitochondrial respiration blocker oligomycin (Oligo), were used as a proxy to monitor the activity of glycolysis to generate ATP. 2-Deoxyglucose (2-DG) and sodium oxamate (SO) were employed to block glycolysis at different steps. SO is an inhibitor of lactate dehydrogenase thus blocking the final step of glycolysis conversion of pyruvate into lactate. Note HK2 KO clones displayed remarkable resistance to decreasing ATP when co-treated with Oligo and BKIDC-1553-N-Me while they were sensitive to 2-DG and SO. **(B)** Western blot validation of HK1 and HK2 deficiency in LNCaP KO clones. GAPDH served as a loading control.

Figure 8. Growth Curves of Prostate Cancer Xenografts Implanted in SCID Mice. The BKIDC-resistant human prostate cancer cell line PC3 and a human patient-derived xenograft (PDX) model (LuCaP 35) were injected subcutaneously in SCID mice. Mice were treated for 4-5 weeks with 20 mg/kg BKIDC-1553 po three times a week. The LuCaP 35 tumors responded to BKIDC-1553 to a similar degree as enzalutamide (Enza) and no decrease was seen in PC3 xenografts. The data are presented as mean ± standard error of mean (SEM) (n=7-10). One-way ANOVA followed by Tukey's test for multiple comparison (LuCaP35) and two-tailed t tests (PC3): *p <0.05, **p <0.01, ns: not significant.

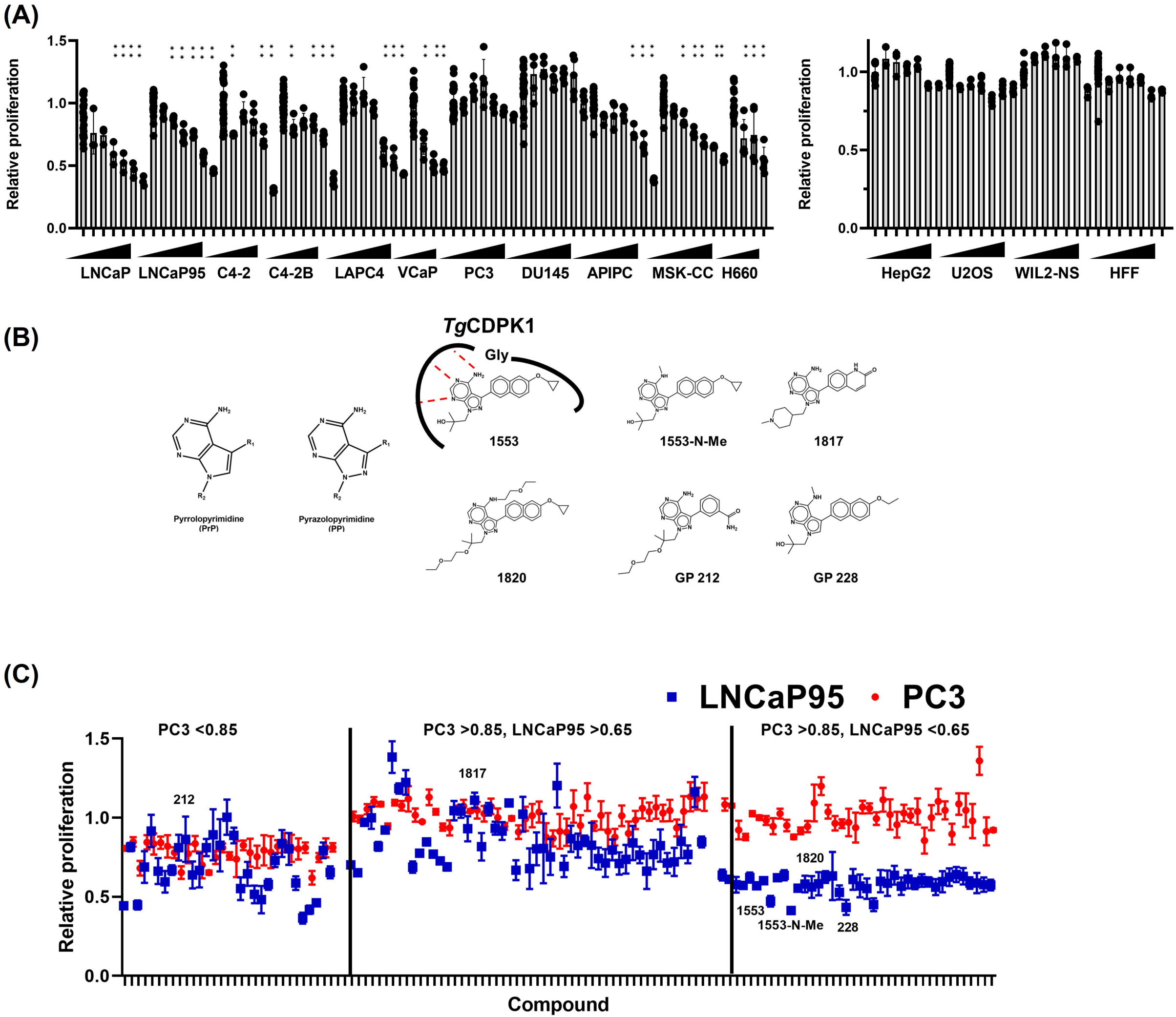
(A)
Relative proliferation
1.5
1.0
0.5
0.0
LNCaP
LNCaP95
C4-2
C4-2B
LAPC4
VCaP
PC3
DU145
APIPC
MSK-CC
H660
HepG2
U2OS
WIL2-NS
HFF
(B)
TgCDPK1
Gly
1553
1553-N-Me
1817
Pyrrolopyrimidine (PrP)
Pyrazolopyrimidine (PP)
1820
GP 212
GP 228
(C)
LNCaP95
PC3
PC3 <0.85
PC3 >0.85, LNCaP95 >0.65
PC3 >0.85, LNCaP95 <0.65
212
1817
1820
1553
1553-N-Me
228
Compound

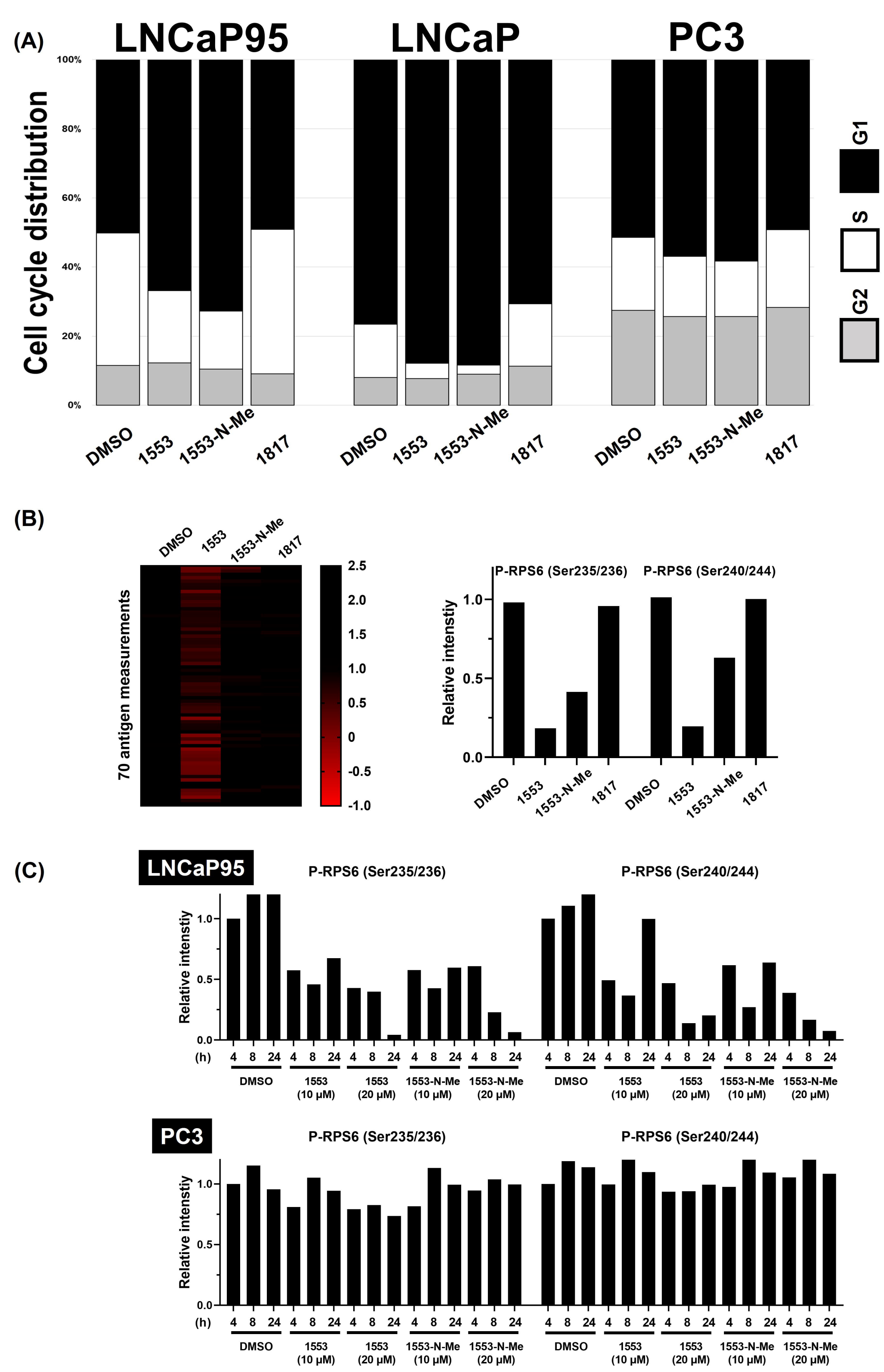
(A)
LNCaP95
LNCaP
PC3
Cell cycle distribution
100%
80%
60%
40%
20%
0%
DMSO
1553
1553-N-Me
1817
G1
S
G2
(B)
70 antigen measurements
2.5
2.0
1.5
1.0
0.5
0
-0.5
-1.0
P-RPS6 (Ser235/236)
P-RPS6 (Ser240/244)
Relative intenstiy
1.0
0.5
0.0
(C)
LNCaP95
PC3
(h)
4 8 24
DMSO
1553 (10 μM)
1553 (20 μM)
1553-N-Me (10 μM)
1553-N-Me (20 μM)

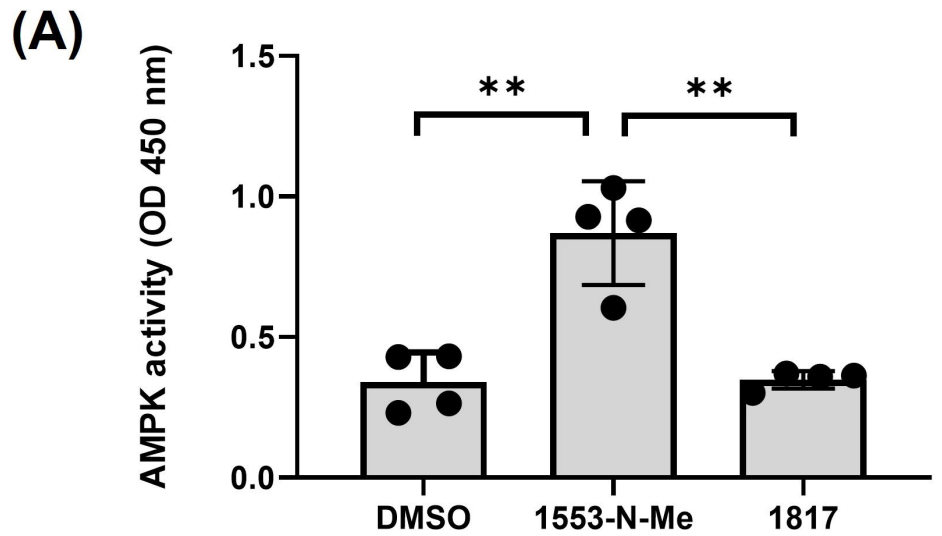
(A)
AMPK activity (OD 450 nm)
1.5
1.0
0.5
0.0
**
**
DMSO
1553-N-Me
1817

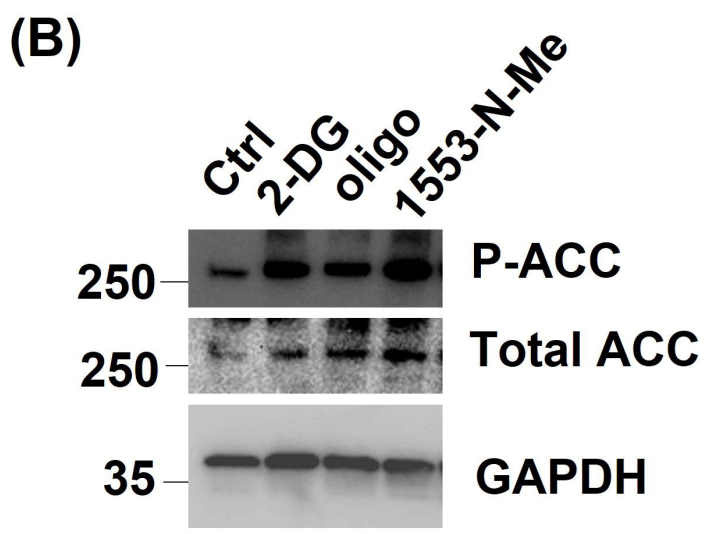
(B)
Ctrl
2-DG
oligo
1553-N-Me
250
P-ACC
250
Total ACC
35
GAPDH

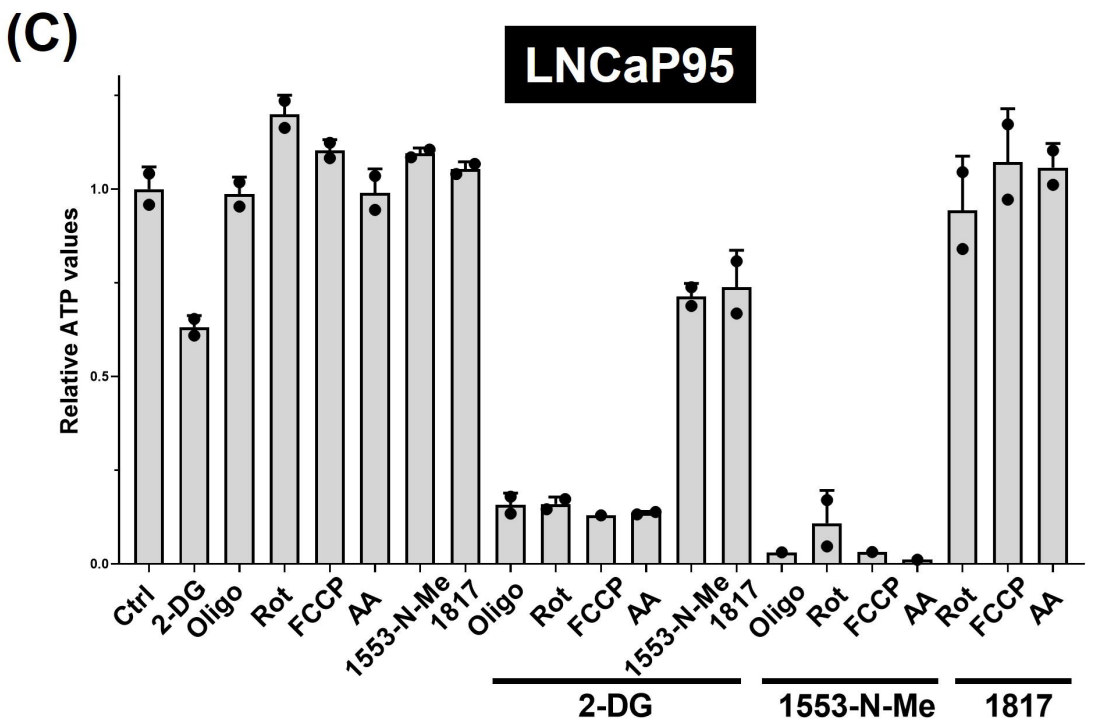
(C)
LNCaP95
Relative ATP values
1.0
0.5
0.0
Ctrl
2-DG
Oligo
Rot
FCCP
AA
1553-N-Me
1817
Oligo
Rot
FCCP
AA
1553-N-Me
1817
Oligo
Rot
FCCP
AA
Rot
FCCP
AA
2-DG
1553-N-Me
1817

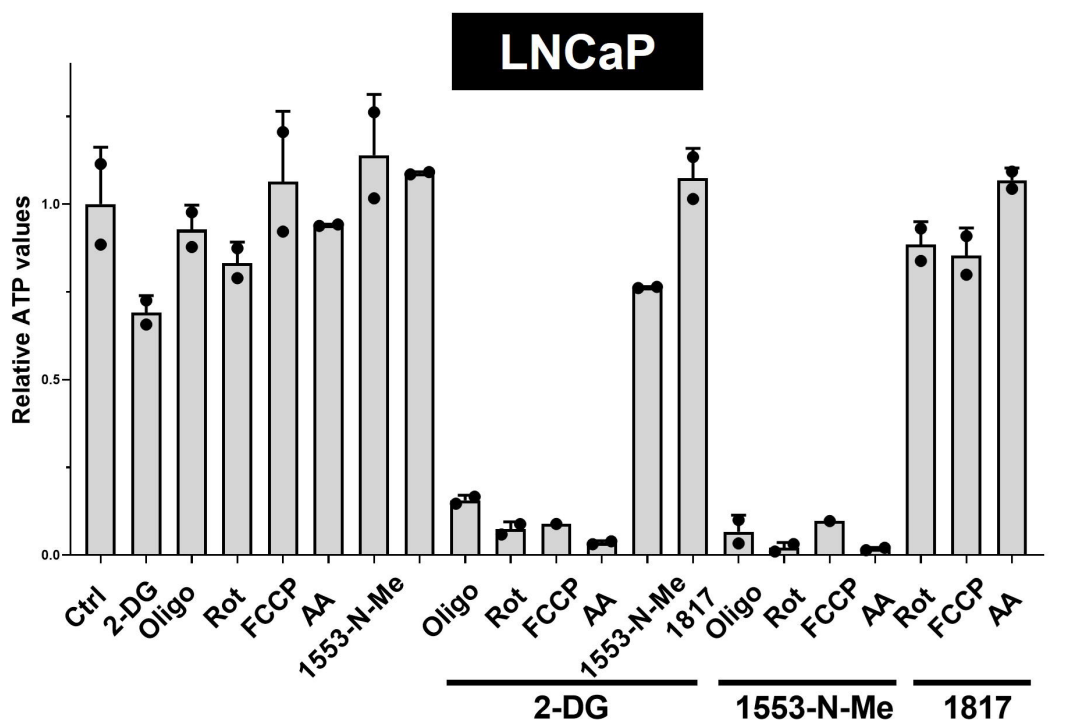
LNCaP
Relative ATP values
1.0
0.5
0.0
Ctrl
2-DG
Oligo
Rot
FCCP
AA
1553-N-Me
Oligo
Rot
FCCP
AA
1553-N-Me
1817
Oligo
Rot
FCCP
AA
Rot
FCCP
AA
2-DG
1553-N-Me
1817

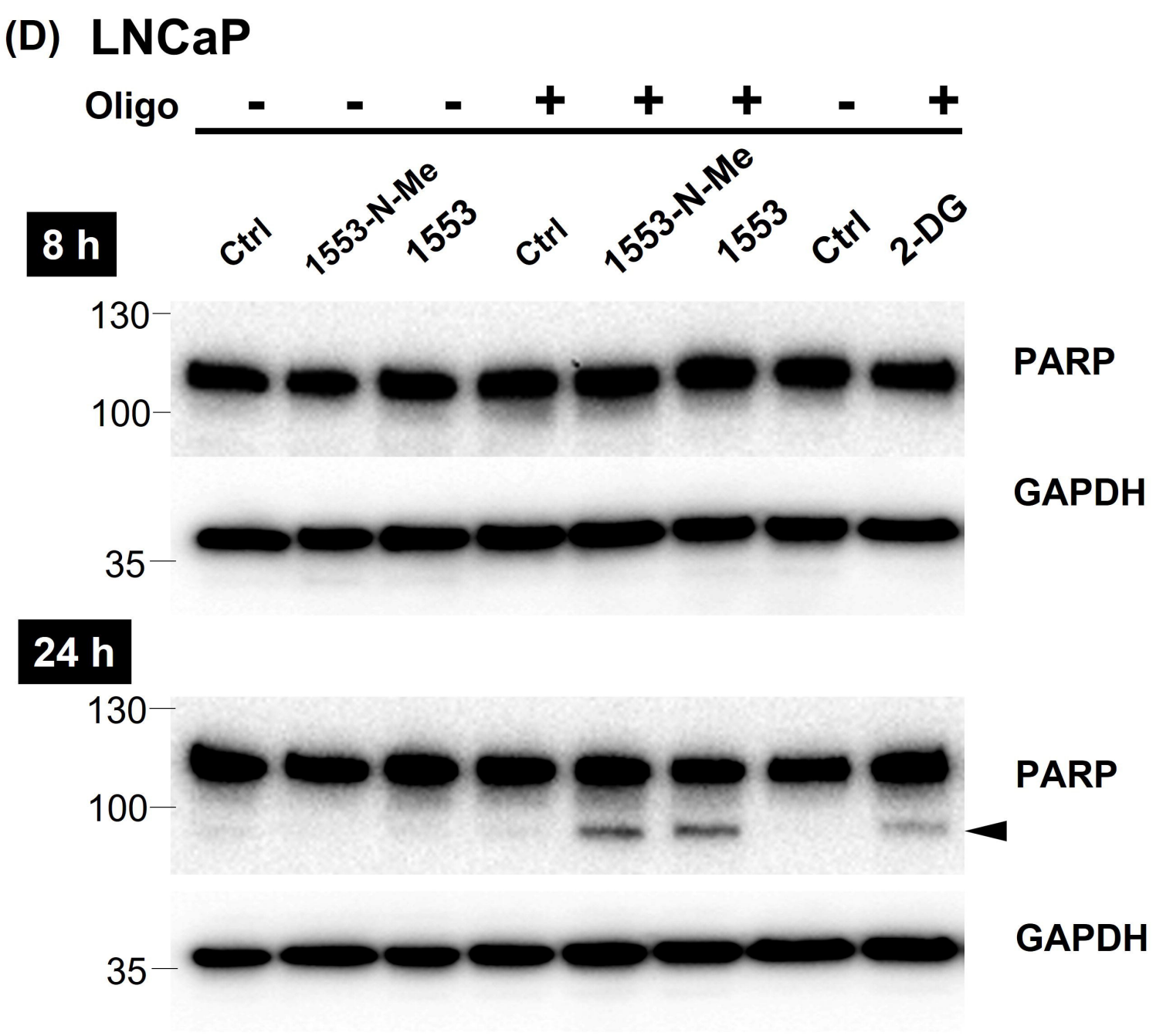
(D) LNCaP
Oligo
-
-
-
+
+
+
-
+
8 h
Ctrl
1553-N-Me
1553
Ctrl
1553-N-Me
1553
Ctrl
2-DG
130
100
PARP
35
GAPDH
24 h
130
100
PARP
35
GAPDH

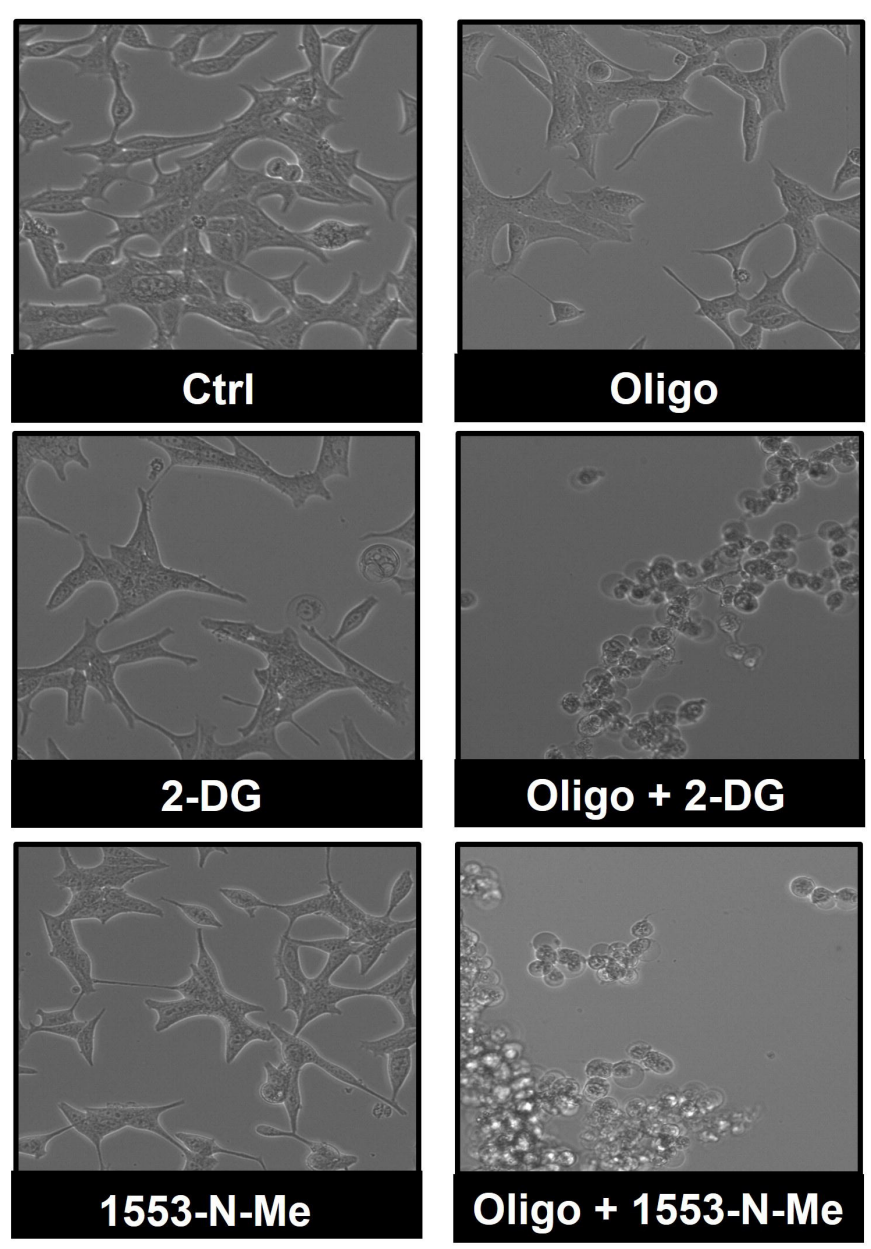
Ctrl
Oligo
2-DG
Oligo + 2-DG
1553-N-Me
Oligo + 1553-N-Me

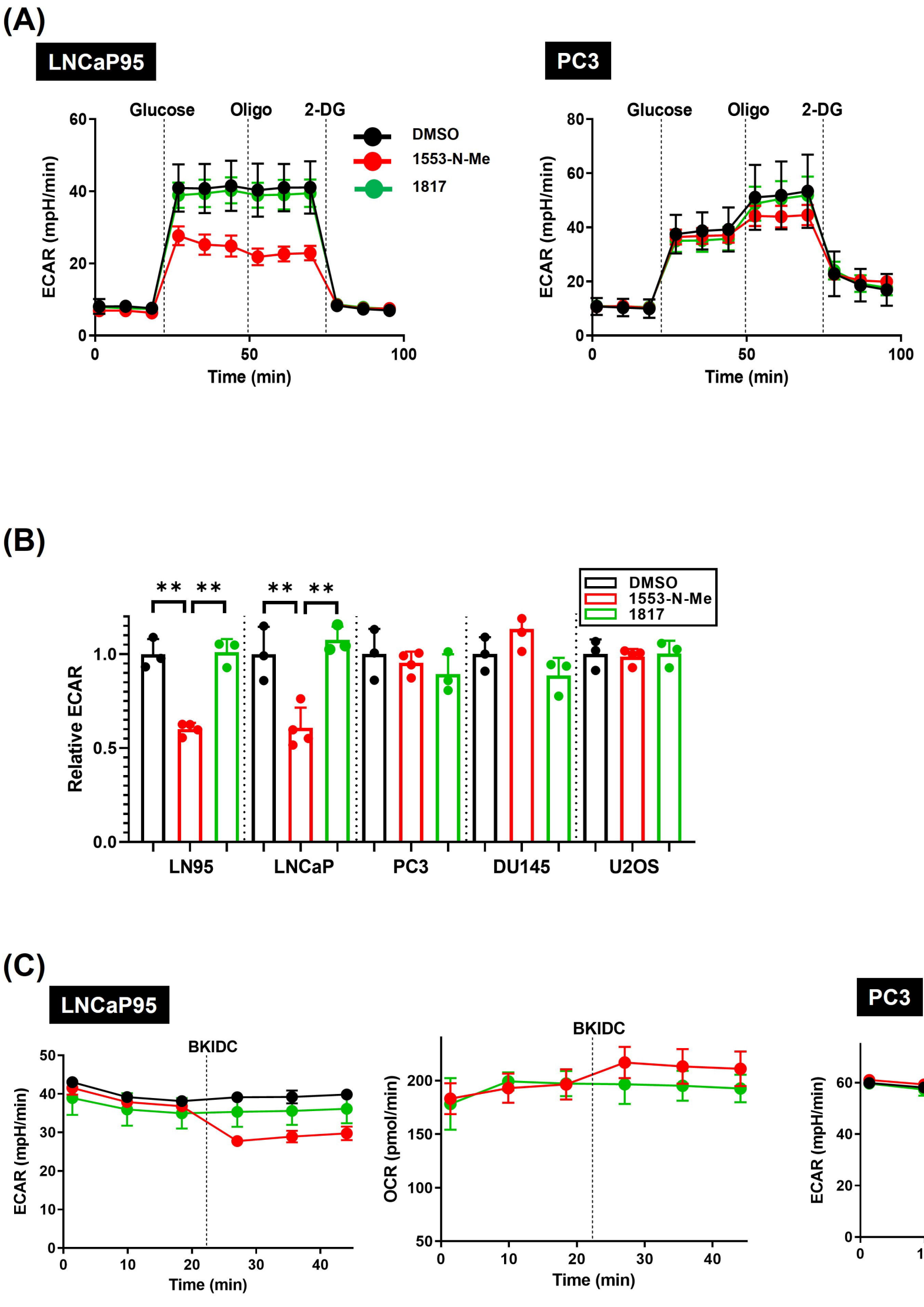
(A)
LNCaP95
PC3
Glucose
Oligo
2-DG
DMSO
1553-N-Me
1817
ECAR (mpH/min)
Time (min)
(B)
Relative ECAR
LN95
LNCaP
PC3
DU145
U2OS
(C)
LNCaP95
PC3
BKIDC
ECAR (mpH/min)
OCR (pmol/min)
Time (min)

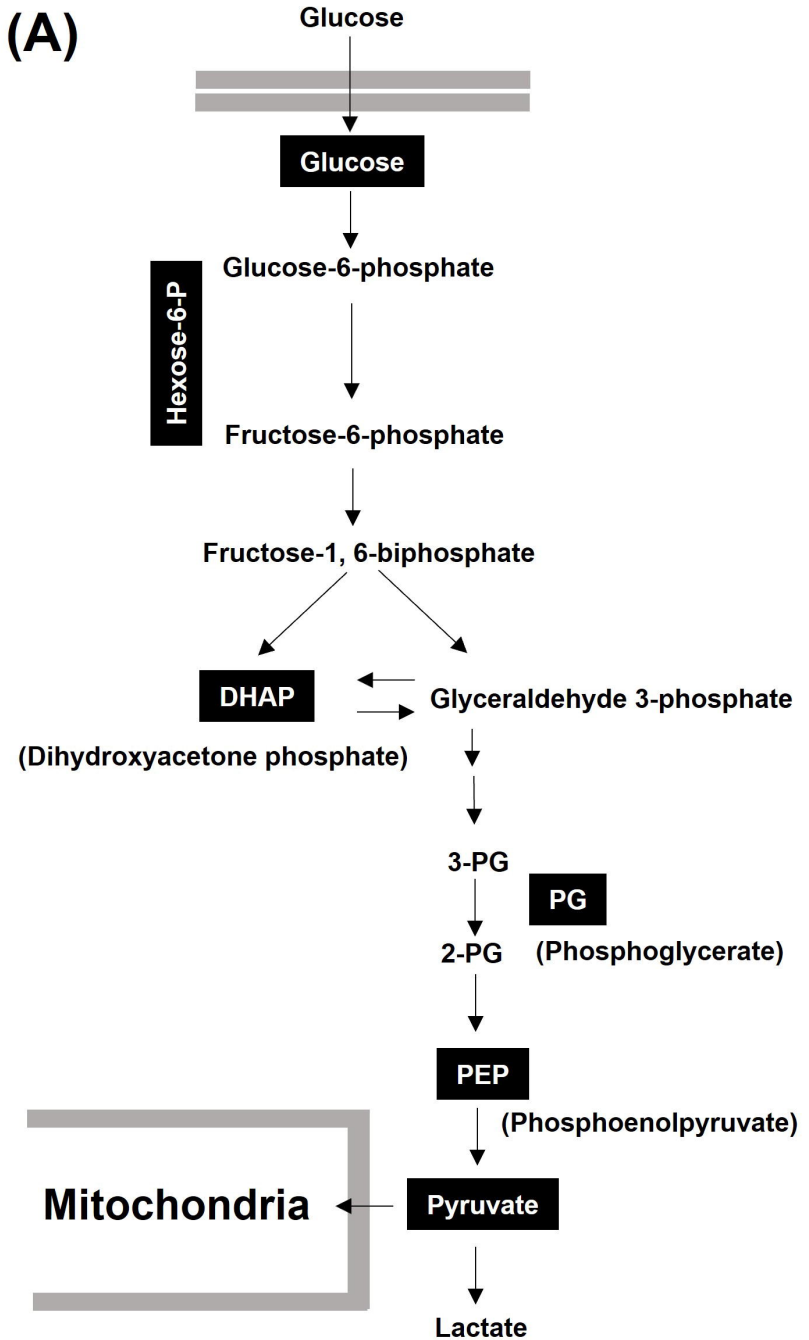
(A)
Glucose
Glucose
Glucose-6-phosphate
Hexose-6-P
Fructose-6-phosphate
Fructose-1, 6-biphosphate
DHAP
Glyceraldehyde 3-phosphate
(Dihydroxyacetone phosphate)
3-PG
PG
2-PG
(Phosphoglycerate)
PEP
(Phosphoenolpyruvate)
Mitochondria
Pyruvate
Lactate

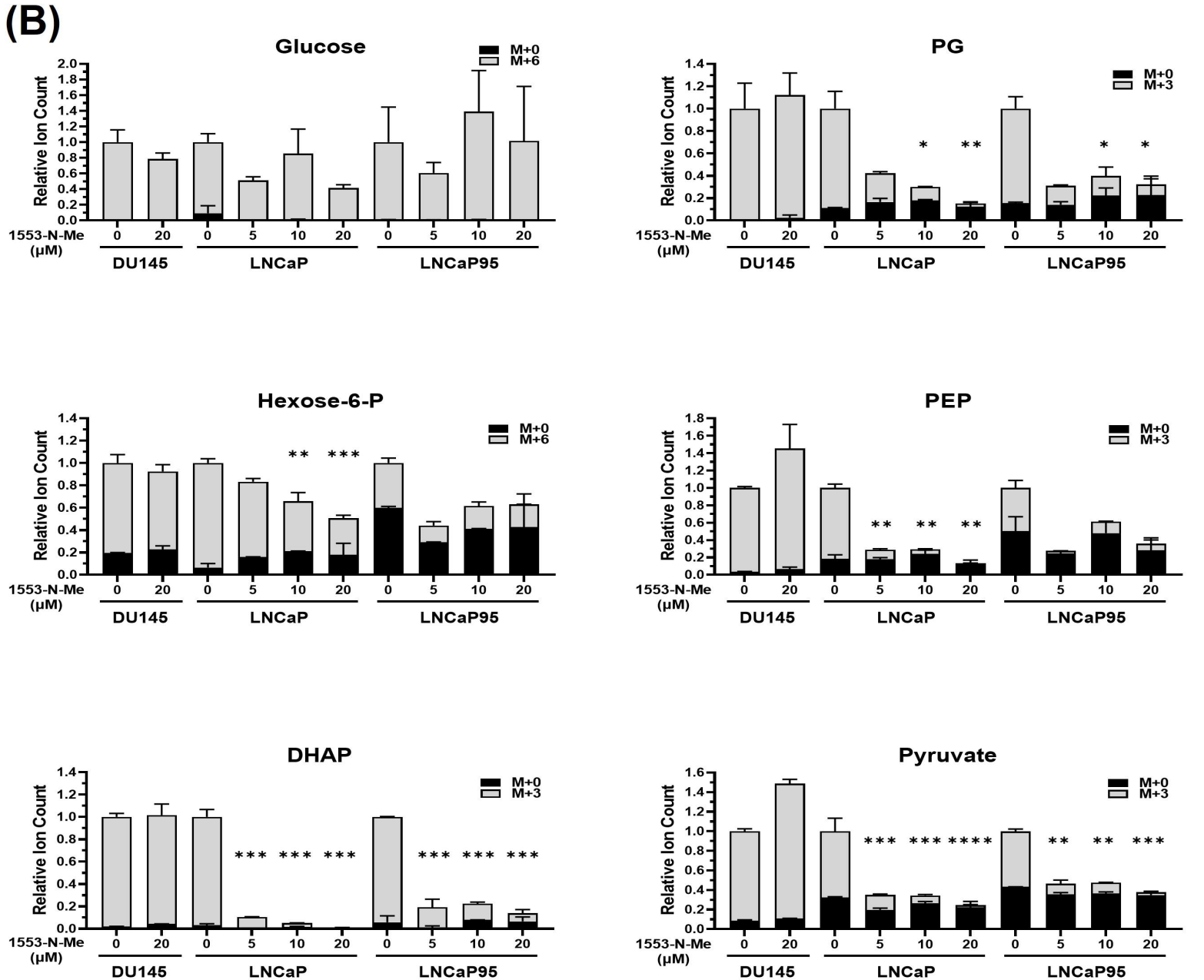
(B)
Glucose
M+0
M+6
PG
M+0
M+3
Hexose-6-P
M+0
M+6
PEP
M+0
M+3
DHAP
M+0
M+3
Pyruvate
M+0
M+3
Relative Ion Count
1553-N-Me (μM)
0 20 0 5 10 20 0 5 10 20
DU145
LNCaP
LNCaP95

(A)

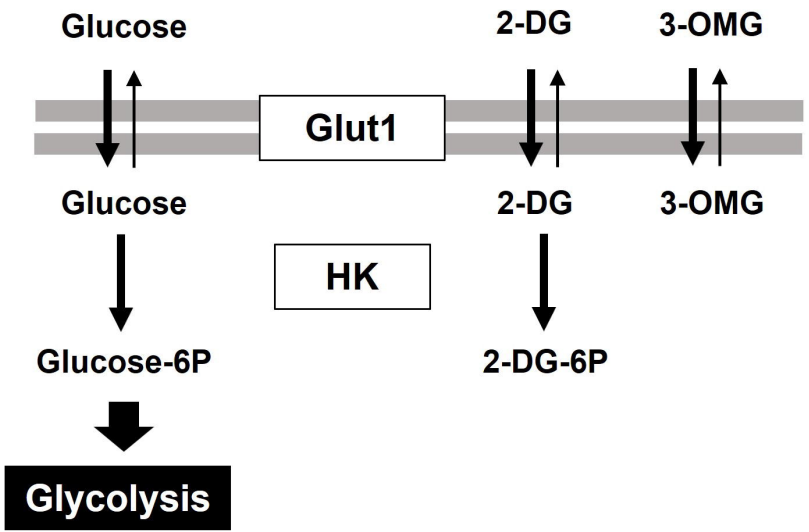
Glucose
2-DG
3-OMG
Glut1
Glucose
2-DG
3-OMG
HK
Glucose-6P
2-DG-6P
Glycolysis

(B)

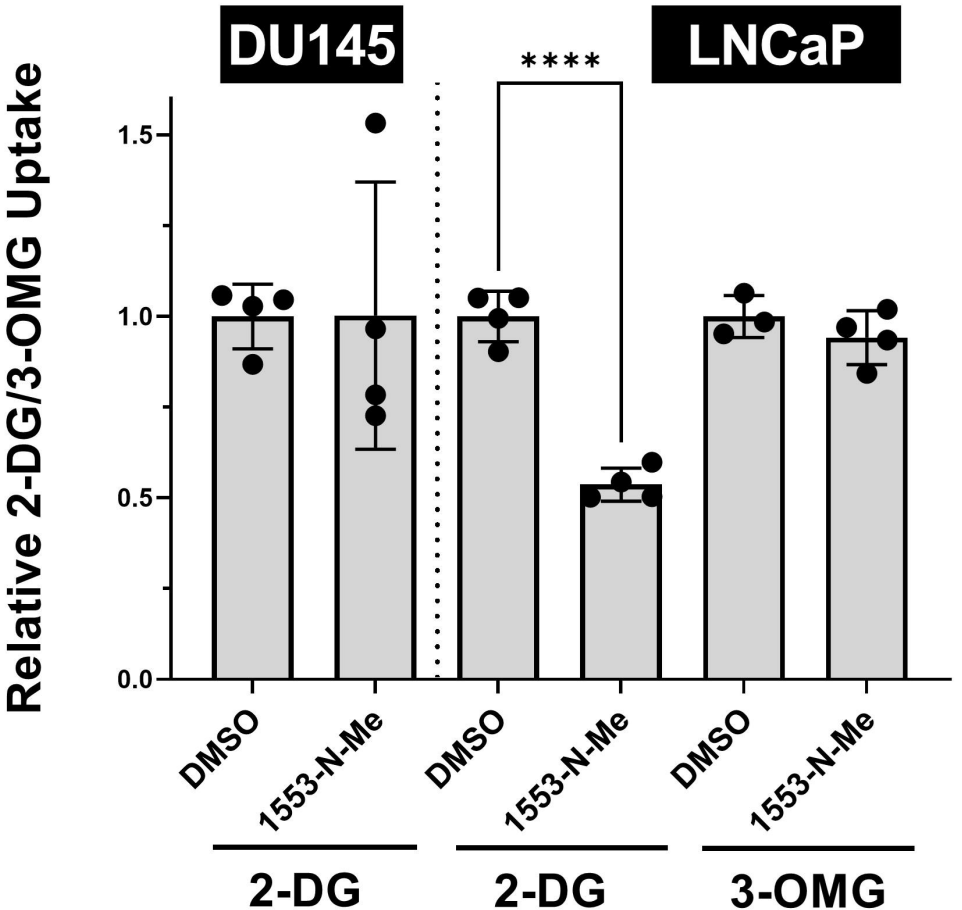
DU145
LNCaP
****
Relative 2-DG/3-OMG Uptake
1.5
1.0
0.5
0.0
DMSO
1553-N-Me
DMSO
1553-N-Me
DMSO
1553-N-Me
2-DG
2-DG
3-OMG

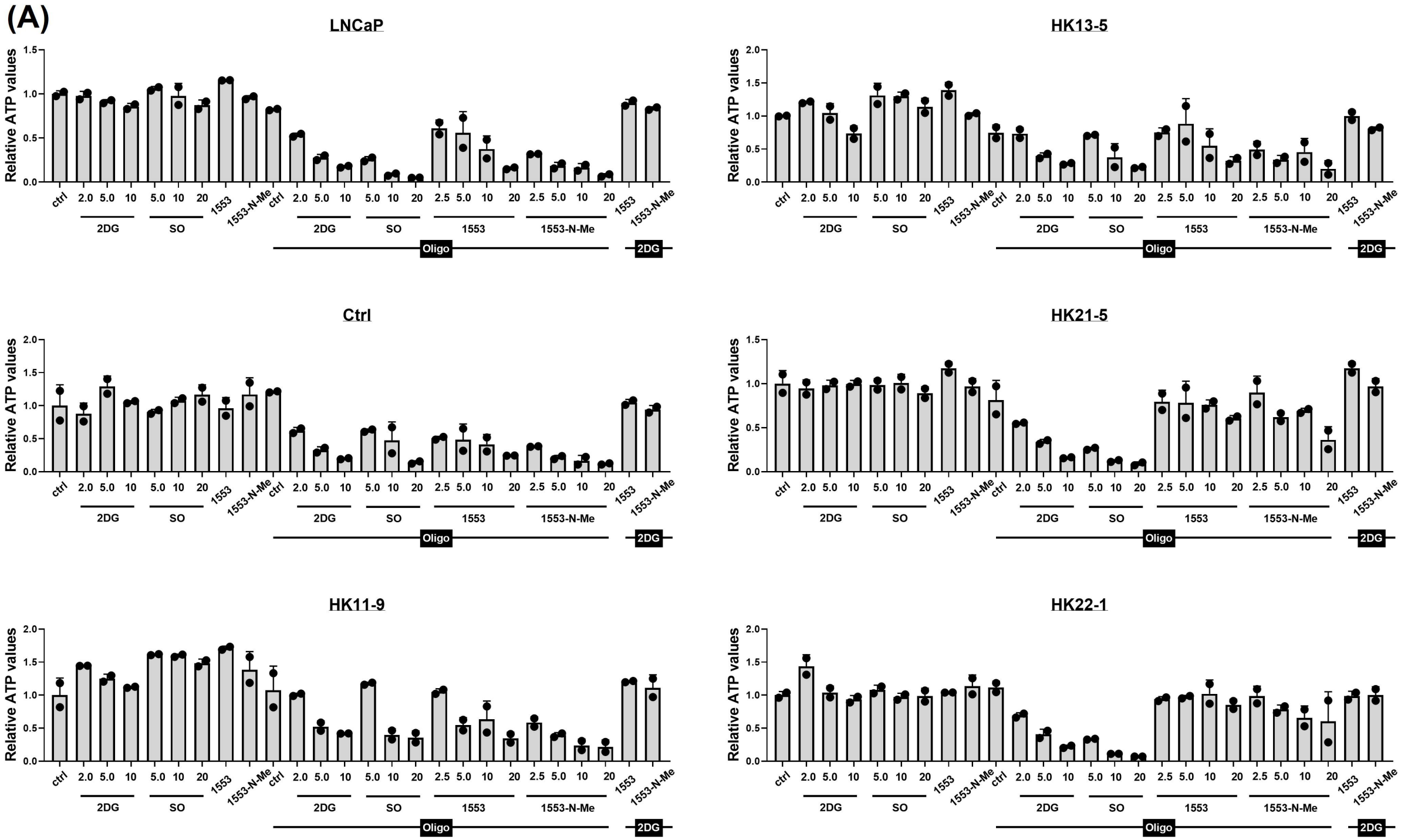
(A)
LNCaP
HK13-5
Ctrl
HK21-5
HK11-9
HK22-1
Relative ATP values
ctrl
2.0
5.0
10
5.0
10
20
1553
1553-N-Me
2.5
2DG
SO
1553
1553-N-Me
Oligo
2DG

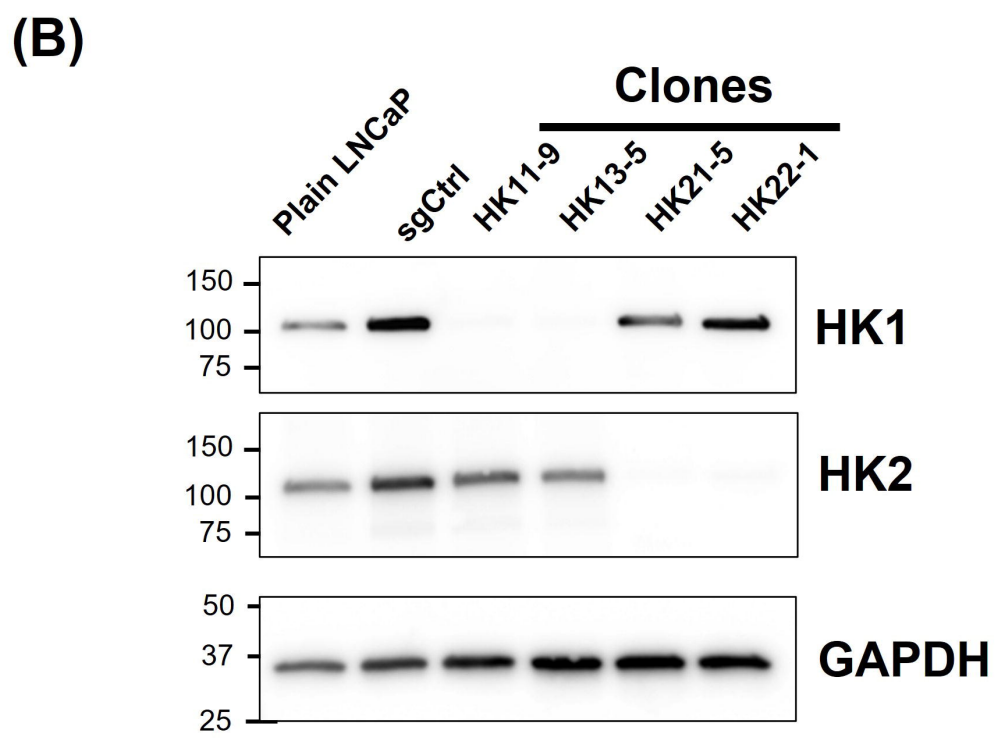
(B)
Clones
Plain LNCaP
sgCtrl
HK11-9
HK13-5
HK21-5
HK22-1
150
100
75
HK1
150
100
75
HK2
50
37
25
GAPDH

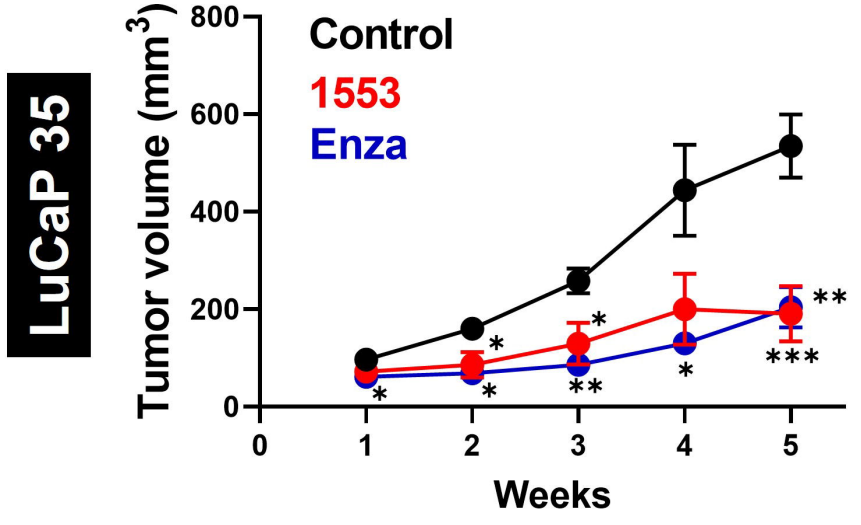
LuCaP 35
Control
1553
Enza
Tumor volume (mm3)
800
600
400
200
0
0
1
2
3
4
5
Weeks
*
*
*
**
*
**
***

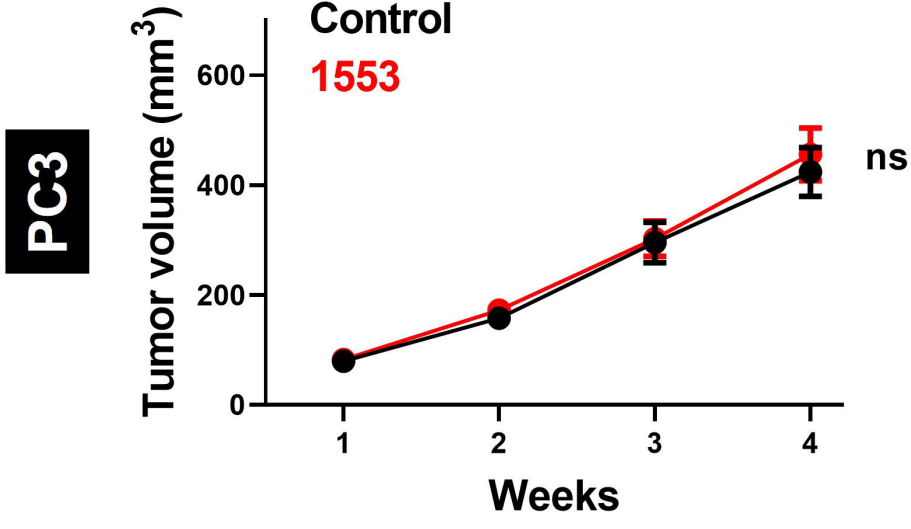
PC3
Control
1553
ns
Tumor volume (mm3)
600
400
200
0
1
2
3
4
Weeks